

REMARKS

This response enclosed with the RCE is offered in reply to the office action mailed December 15, 2005.

In paragraph 3 of the office action, claims 11-16 are rejected under 35 USC 103(a) in view of the Murphy US Patent 5 716 720 taken with the Duhl US Patent 4 719 080 and EP 0 676 489.

Claims 11-16 are believed to distinguish over the '720 patent taken with the '080 patent and EP'489. For example, claim 11 recites a coated article comprising the recited superalloy substrate composition, an outwardly grown diffusion aluminide bondcoat on the substrate, and a ceramic thermal barrier coating disposed on the bondcoat wherein spallation life of the ceramic thermal barrier coating during cyclic oxidation is prolonged.

Applicant's Figures 3, 4, and 5 and specification pages 8-10 illustrate the significant and unexpected prolongation of spallation life of the ceramic thermal barrier coating achieved when the ceramic thermal barrier coating is disposed on the recited outwardly grown diffusion aluminide bondcoat on the recited superalloy substrate composition.

This significant prolongation of spallation life of the thermal barrier coating is unexpected from the oxidation resistance exhibited by the bondcoated alloys shown in Applicant's Figure 2 where the outwardly grown diffusion aluminide bondcoated alloys are designated MDC-150L and the inwardly grown diffusion aluminide bondcoated alloys are designated LDC-2E.

As acknowledged by the examiner, the '720 patent does not disclose or suggest the claimed coated article having the features set forth in claim 11 such that a ceramic thermal barrier coating on a bondcoat exhibits prolongation of spallation life during cyclic oxidation.

Applicant also notes that there is no suggestion whatsoever in the '720 patent that a superalloy composition including hafnium when provided with an outwardly grown diffusion aluminide coating and ceramic thermal barrier coating exhibits a significant and unexpected prolongation of spallation life of the ceramic thermal barrier coating as demonstrated by Applicant's Figures 3, 4, and 5 and specification pages 8-10.

The examiner cites the '080 patent as showing a superalloy composition overlapping that of the pending claims. However, the '080 patent discloses a superalloy composition for making single crystal castings with improved creep strength, thermo-mechanical fatigue behavior, and oxidation resistance uncoated or coated with MCrAlY alloy overlay coating.

The '080 patent nowhere suggests Applicant's recited coated article comprising Applicant's superalloy substrate composition coated with an outwardly grown diffusion aluminide coating and ceramic thermal barrier coating wherein the ceramic thermal barrier coating exhibits a significant and unexpected prolongation of spallation life of the ceramic thermal barrier coating when it is disposed on the recited bondcoat on the recited superalloy substrate composition.

The oxidation resistance test results of the uncoated and MCrAlY alloy overlay coated superalloy of the '080 patent provide no suggestion of Applicant's claimed coated article where the particular combination of the recited superalloy/outwardly grown diffusion aluminide coating/thermal barrier coating result in a significant prolongation of spallation life of the thermal barrier coating.

Neither the '720 patent nor the '080 patent remotely suggests Applicant's coated article comprising the recited superalloy composition coated with an outwardly grown diffusion aluminide coating and ceramic thermal barrier coating exhibiting a significant and unexpected prolongation of spallation life of the ceramic thermal barrier coating by virtue of Applicant's

combination of recited nickel base superalloy/outwardly grown diffusion aluminide bondcoat/thermal barrier coating.

Applicant encloses copies of two technical articles which are not prior art documents, but which are provided for the examiner's review and which Applicant believes rebut the obviousness rejection of claims 11-16. In particular, the first technical article by Clarke and Levi entitled "Materials Design For the Next Generation Thermal Barrier Coatings", Annu. Rev. Mater. Res. 2003, 33:383-417 discusses the status of thermal barrier coating systems comprising a yttria-stabilized zirconia (YSZ) thermal barrier coating deposited onto an oxidation resistant bondcoat applied on a nickel based superalloy component.

On pages 389-390, the article discusses different types of bondcoats and methods of applying them and concludes that "[i]t is uncertain at this time which of these coating types is best for different applications. In large part this is because it is not yet known which combination of materials properties leads to the longest, high temperature life of the coating". On page 390, last paragraph, the article states that "[t]here is substantial circumstantial evidence to suggest that many of the TBC failures are associated with the oxidation of the bondcoat(4). Indeed, a number of manufacturers are believed to use an oxidation criterion as a basis for predicting average life".

As noted above and as is apparent from the above Clarke and Levi technical article, Applicant's significant prolongation of spallation life of the thermal barrier coating is unexpected from the oxidation resistance exhibited by the bondcoated alloys shown in Applicant's Figure 2. The incorrectness of the examiner's hindsight analysis-based rejection is apparent from the first technical article.

The second technical article by Levi entitled "Emerging materials and processes for thermal barrier systems", Current Opinion in Solid State and Materials Science, Volume 8, Issue 1,

January 2004, pages 77-91, emphasizes in Section 2. "The Thermal barrier system" that a system perspective must be taken where interplay between the substrate alloy, bondcoat, and thermal barrier coating must be considered. The incorrectness of the examiner's hindsight analysis-based rejection is also apparent from the second technical article.

As Applicant mentions above, neither the '720 patent nor the '080 patent remotely suggests Applicant's coated article comprising the recited superalloy composition coated with an outwardly grown diffusion aluminide coating and ceramic thermal barrier coating exhibiting a significant and unexpected prolongation of spallation life of the ceramic thermal barrier coating by virtue of Applicant's combination of recited nickel base superalloy composition/outwardly grown diffusion aluminide bondcoat/thermal barrier coating.

The examiner cites EP '489 as showing sulfur levels held to 2 ppm as set forth in Applicant's claim 14. However, EP '489 is otherwise deficient for similar reasons as set forth above for the '080 patent.

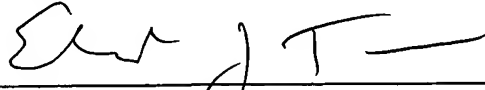
Applicant's believe claim 11 is not suggested by the teachings of the cited references and can only be obtained from the cited references by a prohibited hindsight analysis of the claimed invention. The hindsight nature of the examiner's obviousness rejection is believed to be apparent from the two technical articles, which are enclosed herewith and discussed above and which are subsequent in time to Applicant's claimed priority filing date.

Achievement of a significant and unexpected prolongation of spallation life of a ceramic thermal barrier coating by virtue of Applicant's particular claimed combination of recited nickel base superalloy composition/outwardly grown diffusion aluminide bondcoat/thermal barrier coating of claim 11 is not remotely suggested in the cited references taken alone or together. The same applies to claims 12-16 which recite certain rare earth elements and their concentration, sulfur concentration, and hafnium concentration.

USSN 10/734,078

Applicant believes the pending claims are in condition for allowance and such action is requested.

Respectfully submitted,



Edward J. Timmer Reg. No. 27,402

enclosure: technical articles (2) & Post Card

CERTIFICATE OF MAILING

I hereby certify that this correspondence and enclosures are being deposited with the United States Postal Service as first class mail in an envelope addressed to: Commissioner for Patents  
P.O. Box 1450, Alexandria, VA 22313-1450, on April 14, 2006.



Edward J. Timmer

# MATERIALS DESIGN FOR THE NEXT GENERATION THERMAL BARRIER COATINGS

---

D.R. Clarke and C.G. Levi

*Materials Department, College of Engineering, University of California, Santa Barbara,  
California 93106-5050; email: clarke@engineering.ucsb.edu*

**Key Words** zirconia, materials science, high temperature

■ **Abstract** The emphasis in this short review is to describe the materials issues involved in the development of present thermal barrier coatings and the advances necessary for the next generation, higher temperature capability coatings.

## INTRODUCTION

The development of today's gas turbine engines has been the result of continual improvements in a wide variety of engineering skills including turbine design, combustion, and materials. One measure of the substantial improvements over the past five decades is the increase in the maximum gas temperature at a turbine airfoil afforded by these improvements, as shown in Figure 1. The increase in airfoil temperature has been facilitated by three principal materials developments: dramatic advances in alloy design to produce alloy compositions that are both more creep resistant and oxidation resistant; advances in casting technology that have facilitated not only the casting of large single-crystal superalloy blades and vanes but also the intricate internal channels in the blades to facilitate cooling; and the development of a viable coating technology to deposit a conformal, thermally insulating coating on turbine components. The advances and developments in the first two areas have been reviewed extensively elsewhere (1). Less well known is the development of thermal barrier coatings (TBCs), even though in the last decade their use has enabled a dramatic increase in airfoil temperature, far greater than that enabled by the switch from cast alloy blades to single crystal blades over approximately 30 years.

As originally envisaged, the primary function of a TBC is to provide a low thermal conductivity barrier to heat transfer from the hot gas in the engine to the surface of the coated alloy component, whether in the combustor or the turbine (Figure 2). The TBC allows the turbine designer to increase the gas temperature, and thereby the engine efficiency, without increasing the surface temperature of the alloy. Subsequently, it has been recognized that a TBC also confers additional benefits, for instance, providing protection to rapid thermal transients such as occur

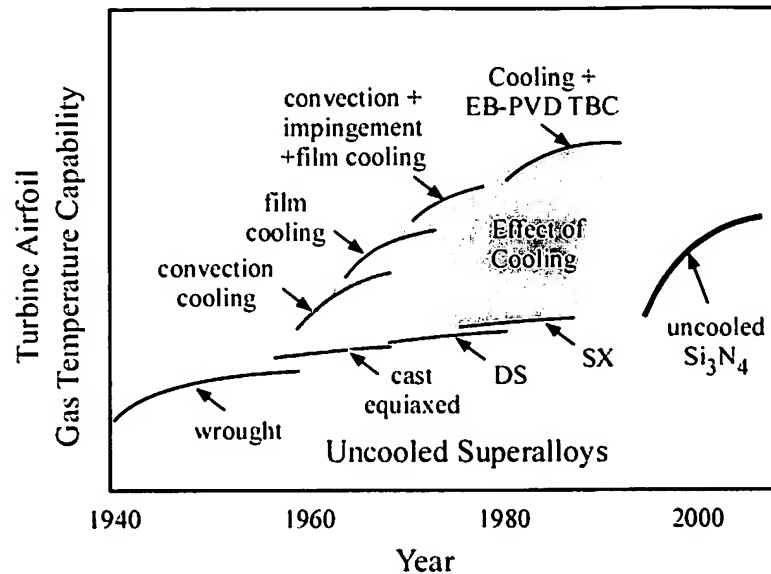


**Figure 1** Increase in turbine airfoil temperature over the last six decades through combinations of materials advances and associated developments in cooling techniques. Since this diagram was constructed, the shaded region has extended to the present year, and the use of uncooled silicon nitride remains for the future.

due to flame out, and as a means to even out local temperature gradients. Indeed, in some cases, the use of a TBC has simplified the design of blades by minimizing thermal distortions of the blade. However, undoubtedly the biggest benefit of TBCs has been to extend the life of alloy components in the hottest sections in an engine by decreasing their surface temperatures.

Present day TBCs generally consist of a yttria-stabilized zirconia (YSZ) coating deposited onto an oxidation-resistant bond-coat alloy that is first applied to a nickel-based superalloy component (Figure 2). In diesel engine applications where the temperatures are usually lower, the YSZ coating is generally applied directly onto the alloy. Two main types of coating are in use. For relatively small components such as blades and vanes in aerospace turbines, the coatings can be applied by electron-beam physical vapor deposition (EB-PVD). For larger components such as the combustion chambers and the blades and vanes of power generation, stationary turbines, the coatings are usually applied by plasma-spraying (PS). In many respects, the choice of materials and their production represent a mature materials technology. While improvements in their capabilities continue, there is a growing realization that new TBC systems will be required for the next generation turbines presently being designed. To set the stage for coming developments, we first review the selection of materials used in present YSZ coatings, some of the new insights that have been gained in understanding how YSZ coatings

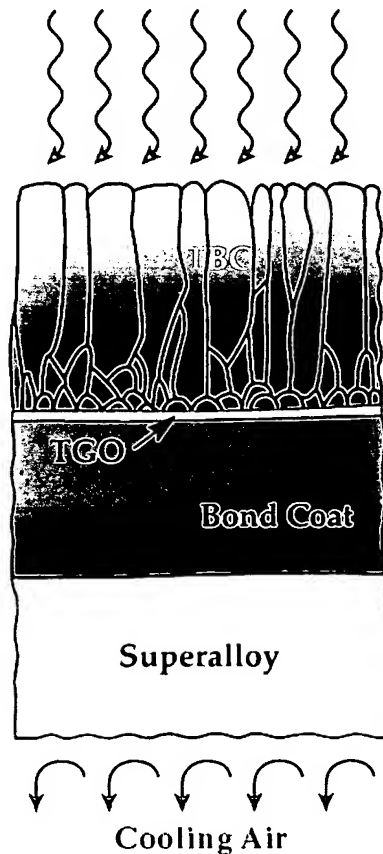


**Figure 2** Schematic illustration of a TBC and the associated bond-coat on a superalloy in a thermal gradient.

fail, and then describe approaches to the development of the next generation TBC systems.

## PRINCIPAL REQUIREMENTS OF A THERMAL BARRIER COATING

The turbine designers' primary requirement of a TBC is that it have a low thermal conductivity and, for rotating components, preferably also a low density to minimize centrifugal loads. At the materials design level this translates into three additional requirements. First, the material must have strain compliance so as to withstand the strains associated with thermal expansion mismatch between the coating and the underlying alloy on thermal cycling. The use cycle, both the maximum temperature and the times at temperature, of course, varies between aircraft and power generation turbines, but nevertheless the coating must accommodate the large strains associated with thermal cycling. The need for strain compliance is illustrated in Figure 3, where the thermal expansion coefficients of zirconia,



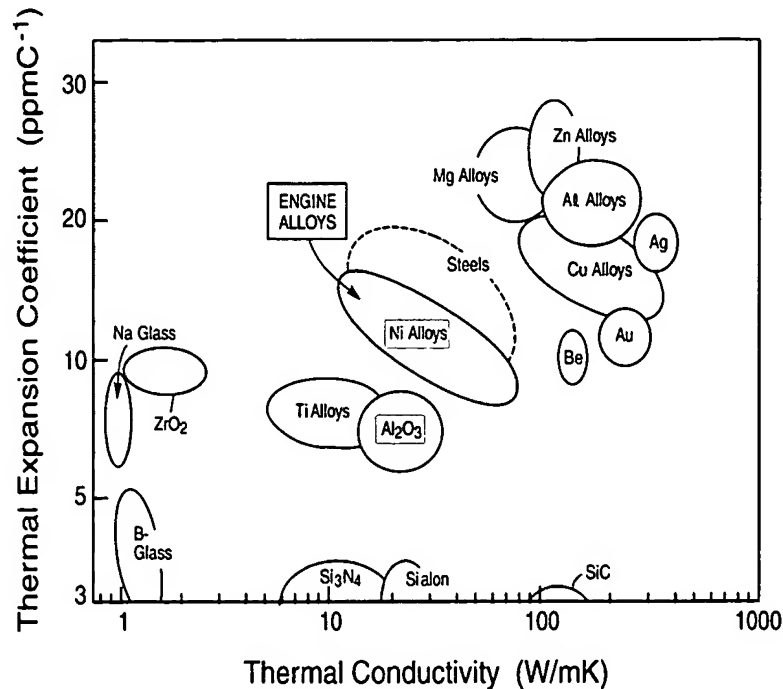


**Figure 3** The thermal expansion coefficients and thermal conductivity of a range of materials illustrating the differences in thermal expansion and conductivity of the principal components in TBC systems.

alumina, and a number of alloys including nickel-based superalloys are cross-plotted against thermal conductivity. In the absence of any strain compliance, for instance due to a decreased elastic modulus, the large elastic mismatch would generate very large stresses and lead to spontaneous failure on cooling. Second, the coating material must exhibit thermodynamic compatibility with the oxide, usually aluminum oxide, formed on the bond-coat alloy at high temperatures. Third, with the continual quest to run engines at higher temperatures and the increasing difficulty of increasing the metal temperature, it is increasingly likely that designers will seek “prime reliant” coatings, namely ones that can be used with assurance that they will not fail. Prime reliant thermal coatings are ones that are necessary to prevent the temperature of the metal from exceeding its maximum temperature, much in the same way that the tiles on the space shuttle prevent the underlying aluminum airframe from being exposed to temperatures in excess of their melting temperature on re-entry.

Because weight is at a premium in aircraft engines, thin coatings with the lowest possible thermal conductivity are required. In contrast, in stationary, ground-based engines where weight is less of a consideration, a desired temperature drop can be

achieved through simply increasing the TBC thickness. In practice, in components in both types of engine, the thickness of the TBC usually is varied from place to place to provide the desired thermal insulation.

Erosion of the coating by both ingested particles, such as sand, from the operating environment and particles that come loose from the combustor liners as it degrades is a perennial source of concern, especially when the particles are large enough to cause impact damage of the coating. In some cases, inborn fine particles, primarily dust and sand, melt into the coating as a wetting silicate while it is hot and can degrade the coating. These silicates, usually variants of Si-Al-Mg-Ca oxides that are the principal elements in sands, are often referred to collectively as CMAS.

A recently recognized requirement of many materials exposed to high temperatures in gas turbines is a long-term stability in the presence of steam. This is partly a direct result of the generation of water during the combustion process, but in a number of designs it is a consequence of the use of steam injection to enhance turbine efficiency. Little is known about the effects of long-term exposure to steam on turbine materials. However, tests have revealed that many silicon-based compounds, including SiC, are unstable to the formation of volatile SiO, which results in the slow retraction of the material as evidenced by the reduction in thickness of components over long operating periods. This active oxidation and evaporation phenomenon precludes the use of silicon compounds in coatings unless protected by another coating.

More difficult to design against are the effects of corrosion, especially airborne species and those, such as sulfur and vanadium, in the fuel itself. The majority of land-based turbines operate on natural gas, but there is increasing interest in using alternative fuels, such as coal gas, that are much dirtier. The consequences of using such alternative fuels and their effects on coatings are only now beginning to be investigated.

## THE THERMAL BARRIER COATING SYSTEM

From a materials engineering perspective, it is necessary to consider the TBC as an integrated materials system rather than simply a thermally insulating material coating on a structural alloy component. A representative cross-section of a commercial coating, shown in Figure 4, illustrates the multilayered nature of a coating after high-temperature exposure. There are three principal layers in addition to the superalloy and the low-conductivity coating. Between the alloy and the coating is the bond-coat, so called because in the initial development stages in producing a viable coating, it was found that the superalloy had to be first covered with a bond-coat to ensure that the YSZ coating remained adherent upon oxidation. Between the bond-coat and the YSZ coating—sometimes referred to as the overcoat—is the oxide formed during high-temperature exposure. Finally, during the formation of the bond-coat and the YSZ coating as well as subsequently during use, a reaction layer forms as a result of inter-diffusion between the bond-coat and the superalloy.

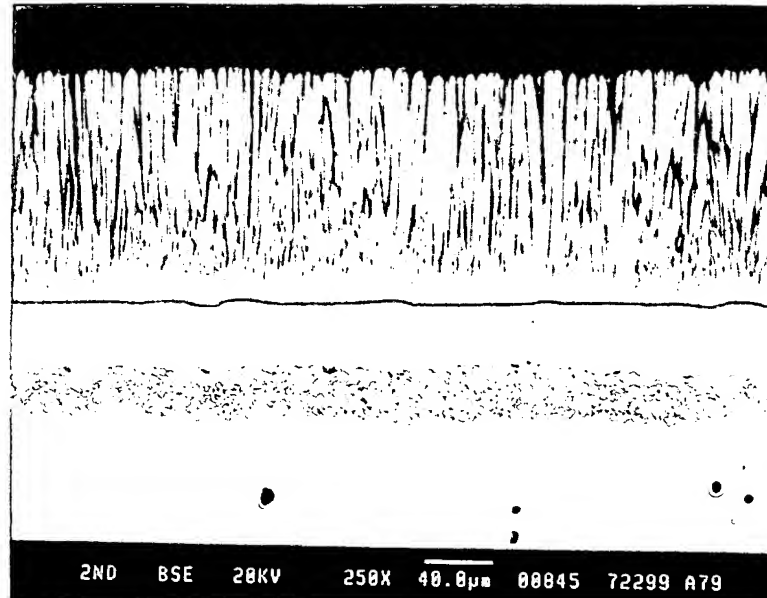


**Figure 4** Cross-section of a TBC deposited by electron beam evaporation. Note the columnar microstructure of the zirconia coating. The white band is a reaction layer formed by interdiffusion during use between the Al-rich bond-coat above and the Ni-rich superalloy, below. The thermally grown oxide (TGO) is too thin to be discernible in this micrograph.

In practice, as mentioned above, there are two distinct types of zirconia coatings reflecting different approaches to creating the strain compliance essential to withstand thermal cycling. The two types of coatings are EB-PVD coatings and plasma-sprayed coatings. In EB-PVD coatings, the lateral strain compliance results from the columnar structure and inter-columnar gaps produced by rotation of the component during deposition. The columnar structure can be seen in the micrograph of Figure 4. Transmission electron microscopy reveals that the individual columns also contain microscopic porosity that reduces the thermal conductivity of the coating. In plasma-sprayed coatings, the lateral strain compliance and reduced thermal conductivity is conferred by the incorporation of porosity between “splats” of successively deposited material. This porosity is illustrated in Figure 5, where the splats in a plasma spray bond coat have preferentially oxidized and consequentially appear as dark veins.

Two major classes of bond-coat alloys have also evolved over the years, but both were developed to form an aluminum oxide ( $\alpha$ - $\text{Al}_2\text{O}_3$ ) on exposure to air at high temperatures. This is important for several reasons. One is that  $\text{Al}_2\text{O}_3$  is phase compatible with YSZ, ensuring long-term thermodynamic stability of the coating. Uncoated, the majority of nickel-based superalloys form complex,

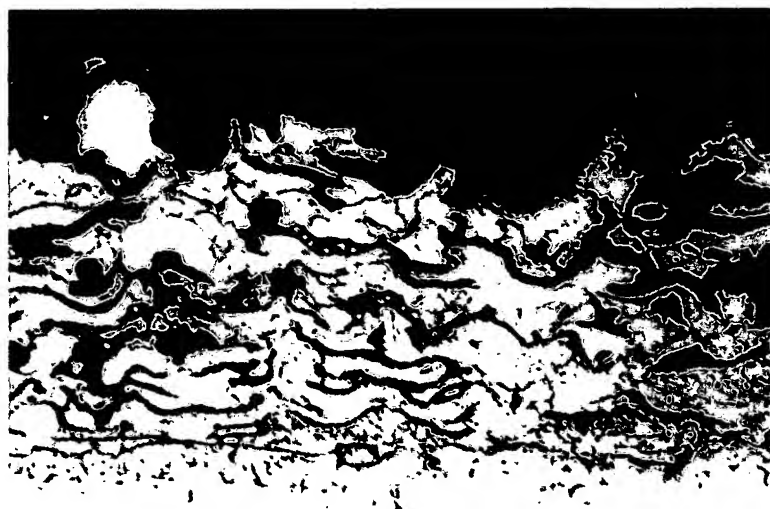


**Figure 5** Cross-section of a TBC deposited by plasma-spraying. The plate-like porosity is evident in the coating as the dark veins in the center of the micrograph.

multilayered nickel oxide, nickel-chromium spinels and chromium oxide, in addition to alumina, and these are not thermodynamically stable with YSZ (2). Furthermore, alumina is usually considered to be the slowest growing high-temperature oxide on account of it having the smallest oxygen diffusivity (3). The rationale for the selection of bond-coat alloys is really a subject of another review, but the bond-coat has to perform a number of disparate functions. It must provide a bond between the deposited TBC and the underlying alloy. In the early days of TBC development, the bonding to the alloy was a major concern, particularly plasma-sprayed, hence the term bond-coat. Because zirconia is a fast-ion oxygen conductor, the bond-coat must also be able to form a protective, stable, and slow-growing oxide to prevent oxidative attack of the alloy. As is described below, one of the principal forms of failure is associated with failure of the protective aluminium oxide. The bond-coat must also have sufficient morphological stability so that on heating and cooling, as well as at high temperature, it does not distort and introduce incompatibilities that can also cause the introduction of interface defects.

The two classes of bond-coat alloys that have been developed are the platinum-modified nickel aluminide (PtNiAl) and MCrAlY alloys (M here refers to one or more of the elements Co, Ni, and Fe). The selection of these two classes of alloys is largely based on their prior use as oxidation- and corrosion-resistant coatings for protecting high-temperature alloys before the advent of TBCs. For instance, the

PtNiAl was originally developed as an alternative oxidation-resistant coating for protecting alloys at higher-temperature operation than the MCrAlY alloys available at the time.

Different methods of applying the bond-coat alloys have been developed largely to meet production goals. Typically, PtNiAl bond-coats are formed by first electrodepositing Pt onto the superalloy component and then annealing it in an aluminum-rich vapor atmosphere. In this second step, aluminum diffuses into the surface of the alloy while nickel diffuses out where it reacts with the aluminum and platinum to form the PtNiAl aluminide coating. Depending on the quality of the coating required, the aluminum is provided in a pack-process or in a CVD reactor from an  $\text{AlCl}_3$  source. In contrast, the MCrAlY coatings are commonly deposited by one of a number of variants of plasma-spraying. These processes are particularly attractive for coating large components and are, of course, cheaper than EB deposition. Also, as plasma-spraying does not involve a diffusion process, thicker bond-coats can be deposited than with the aluminizing process used to form the PtNiAl bond coats.

It remains uncertain at this time which of these coating types is best for different applications. In large part this is because it is not yet known which combination of materials properties leads to the longest, high-temperature life of the coating. To provide the largest reservoir of aluminum one would expect that the thicker the bond-coat and the higher its aluminum content the better. However, one would also expect that the bond-coat should have as large a yield stress as possible at high temperature with as closely matched thermal expansion mismatch with the superalloy as possible to avoid thermal expansion mismatch stresses on thermal cycling.

## FAILURE MECHANISMS

Investigation of the ways in which present YSZ coatings fail has provided considerable insight into the underlying mechanisms that limit coating life. Although, as with failure analysis in other areas of complex material systems, there are many complications, the findings nevertheless point toward methods of producing coatings that can withstand longer lives at temperature and higher use temperatures. One of the chronic problems is that the life of present TBC coatings invariably shows a wide distribution, with a high proportion of the population clustered about a median value but with a significant proportion failing at much earlier times.

There is substantial circumstantial evidence to suggest that many of the TBC failures are associated with the oxidation of the bond-coat (4). Indeed, a number of manufacturers are believed to use an oxidation criterion as a basis for predicting average life. One such criterion is the combination of time and temperature to lead to a critical thickness of the TGO<sup>1</sup>. Another, embodied in the Coatlife software, is an aluminum depletion criterion based on the combined time and temperature

<sup>1</sup>The concept of a critical thickness, of the order of 6  $\mu\text{m}$  at 1100°C, appears to have originated from observations of coatings that failed under isothermal testing conditions.

for the concentration of aluminum at the bond-coat surface to fall below a critical value. In the case of MCrAlY bond-coats, the rationale for this is that when the Al concentration falls to  $\sim 8$  a/o, aluminum oxide is no longer the thermodynamic preferred phase and other oxides, notably spinels, form (5). These other oxides do not form such a protective scale, and consequently the alloy oxidizes faster. In addition, the formation of these oxides is associated with an increase in volume that can be disruptive and possibly have lower fracture energies, although this has yet to be unequivocally demonstrated. Nevertheless, there are reports that when the bond-coat is porous, and at low-oxidation temperatures, failure follows such aluminum depletion (6).

Although related to the oxidation behavior of the bond-coat, neither the concept of a critical thickness nor aluminum depletion can account for the wide distribution in failure lives, especially under thermal cycling conditions. Indeed, in the majority of materials examined after failures above about 1000°C, the aluminum concentration, although depleted somewhat, has not fallen to the critical value (7). Similarly, the short-lived coatings have failed before the TGO thickness has reached the thickness of its counterparts that have shown the longest lives. Together these findings indicate that failure occurs due to extrinsic factors arising during oxidation.

The prevailing mode of failure is one in which part of the coating buckles and spalls away from the alloy, typically on cooling down to room temperature (8, 9). A typical buckling failure, in this case nucleated from the edge of a test coupon, is illustrated in Figure 6. Such buckling and subsequent spallation is a common mode of failure of all films and coatings under compression, generally associated with the development of compressive residual stresses in the coatings as a result of the difference in thermal expansion coefficient between the coating and the underlying alloy. The mechanics of the failure by buckling of a thin, elastically isotropic film under compression from a flat surface is well understood (10), provided an unbonded region of a critical size,  $d_b$ , exists at the interface (Figure 7). For a fixed film thickness and residual stress, the stress at which buckling will occur is given by the relation:

$$\sigma/E = 4.8 \left( \frac{h}{d_b} \right)^2. \quad 1.$$

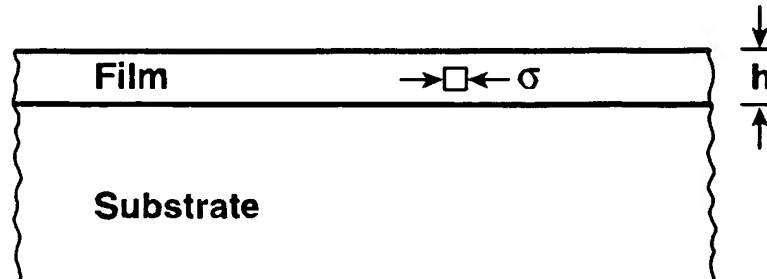
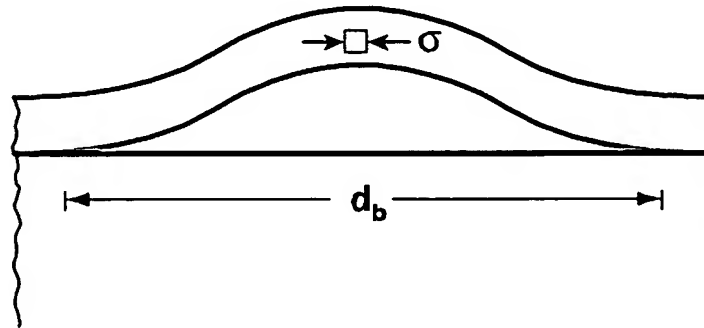
Thin film buckling is entirely analogous to the standard Euler buckling condition of a column—a bifurcation phenomenon. The striking feature of this relation is that the flaw size depends linearly on the thickness of the film.<sup>2</sup> Since even the thinnest of TBC is over 100  $\mu\text{m}$  thick, the critical size to which an interface flaw must grow before buckling can occur can be several millimeters. As interface separations of this large size are not usually present after coating, one of the major unresolved

<sup>2</sup>Because they are designed to have in-plane strain compliance, TBCs are not usually isotropic elastic solids. The buckling condition is modified from that in Equation 1 to account for the elastic anisotropy.



**Figure 6** (Top) Incipient buckling of a TBC coating viewed under reflected light. (Bottom) The failure surface revealed by spallation of the TBC consists of a mixture of local failure between the TGO and the bond-coat (*appearing dark*) and in the TBC itself (*light regions*).

questions is how interface separations first form and then grow to such a large size. Such progressive failure consisting of nucleation of local interface separation and their subsequent growth has indeed been observed (11). Recent mechanics calculations have shown that interface perturbations from flatness can decrease the critical size at which buckles can initiate and then grow in size to form a spall

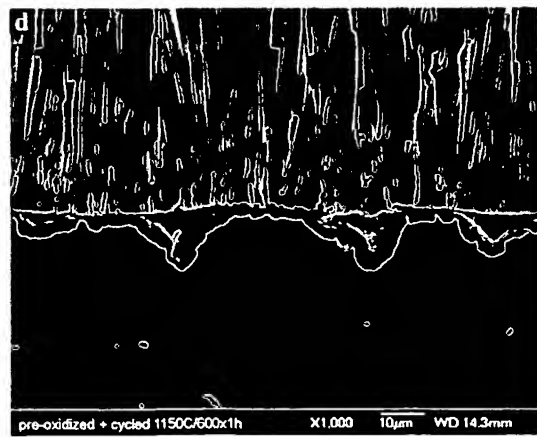
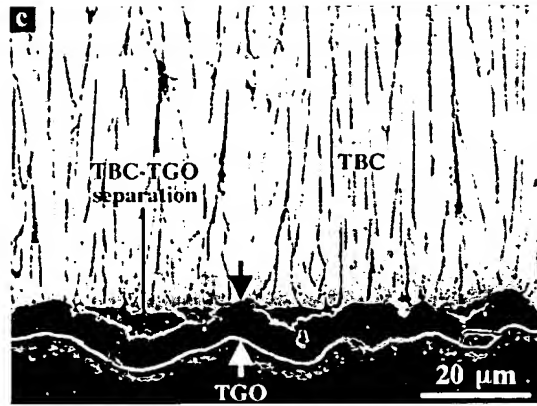
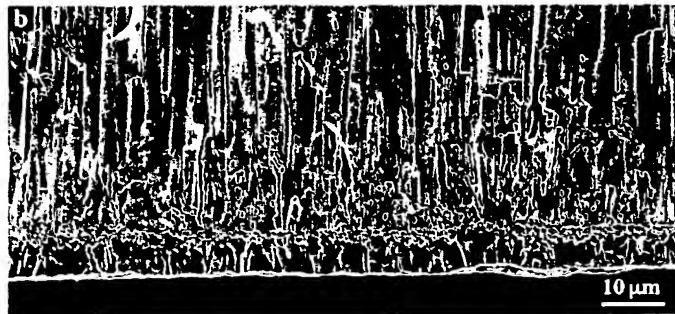
**Before:****After:**

**Figure 7** Schematic illustration of the buckling of a compressed film above a pre-existing defect of diameter  $d_b$ .

(12). Nevertheless, localized flaws must first initiate and then grow for spallation failure to occur. Understanding the nucleation of these flaws, their growth, and progressive linking together is essential before realistic models for predicting life can be developed.

Insight into the formation of flaws comes from microstructural examination of coating cross-sections after high-temperature exposure but prior to spallation. Four examples are shown in Figure 8, each from a YSZ TBC-coated PtNiAl bond-coat (13). In each case, the coating was deposited conformally onto the surface of a flat bond-coat so that the coating/bond-coat interface was initially flat and intact. As three of the micrographs illustrate, the surface of the bond-coat roughens and separations form with the TBC even though the bottom surface of the TBC remains flat. These separations are the interface flaws that progressively grow in size and link together with adjacent ones to allow buckling and spallation (9, 11). Roughening is more pronounced with thermal cycling but also occurs, albeit more slowly, on isothermal exposures (14). The growth of these separations with thermal cycling can now be monitored by luminescence piezospectroscopy, as described





in the next section, which suggests that it has the potential to be used as a viable NDE tool (11, 15).

The micrographs in Figure 8 raise the question as to the underlying mechanisms responsible for the observed roughening. At least two new mechanisms have now been identified that can lead to such roughening. The roughening has been attributed to a "ratcheting" phenomenon motivated by the lateral compressive stress in the growing TGO and facilitated by thermal cycling (9). Measurements indicate that as the TGO grows in thickness with oxidation, it also concurrently develops a compressive stress (16, 17). If it were free to expand it would decrease its compressive stress but because it is attached to the bond-coat, the only way in which it can decrease its elastic strain energy is by undulating (Figure 9). In this way, its length increases and it remains attached to the alloy. This undulation requires the alloy to deform to accommodate the undulation, and the oxide must also deform concurrently. According to the ratcheting mechanism, this accommodation is by plastic deformation of both the TGO and bond-coat during thermal cycling. As the lateral growth of the thickening oxide continues during the high-temperature portion of the thermal cycles, it continues to generate compressive stress that is relaxed by ratcheting during the thermal cycle so the process is ongoing. Many of the essential features of the mechanism have been substantiated by finite element computations (18) and are consistent with observations of the increase in length of the TGO as the surfaces roughen.

Another new mechanism shown to cause roughening is the surface displacement associated with volumetric changes in the bond-coat as aluminum depletion occurs. This roughening is illustrated in Figure 10, together with etched cross-sections revealing the presence of both  $\gamma'$  and  $\beta$  phases in the bond-coat (14). After aluminizing and after YSZ deposition, the PtNiAl bond-coat is chemically homogeneous and has the  $\beta$ -NiAl (B2) crystal structure. After high-temperature exposure, the initially flat bond-coat is rumpled and etching reveals that the bond-coat has partially transformed to  $\gamma'$ -Ni<sub>3</sub>Al. In addition, the remaining  $\beta$ -NiAl phase regions often have the characteristic lath structure of a martensite. These two observations can be understood as being the result of aluminum depletion from the bond-coat and concurrent enrichment of nickel from the underlying superalloy, a classic example of interdiffusion. This change in composition is illustrated using the binary NiAl diagram in Figure 11. As aluminum is depleted, the average composition of the bond-coat becomes increasingly enriched in nickel until reaching

---

**Figure 8** Cross-section of four TBCs illustrating different forms of the local separation between the TBC and the bond-coat after thermal cycling. In each case, the coating was deposited conformally on the bond-coat so interface separations such as these indicate that the underlying bond-coat has changed its surface morphology during high-temperature exposure and thermal cycling. In example (b), no separation has occurred and it exhibits the longest life.

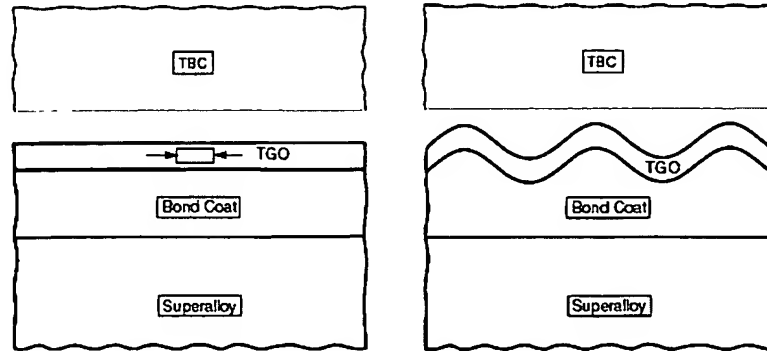


**Figure 9** Schematic illustration of how an initially flat but compressed film (*left*) can lower its elastic strain energy by rumpling (*right*). The amplitude of rumpling is enhanced by thermal cycling and can cause interface separation if a superimposed coating cannot deform to follow the displacements of the film.

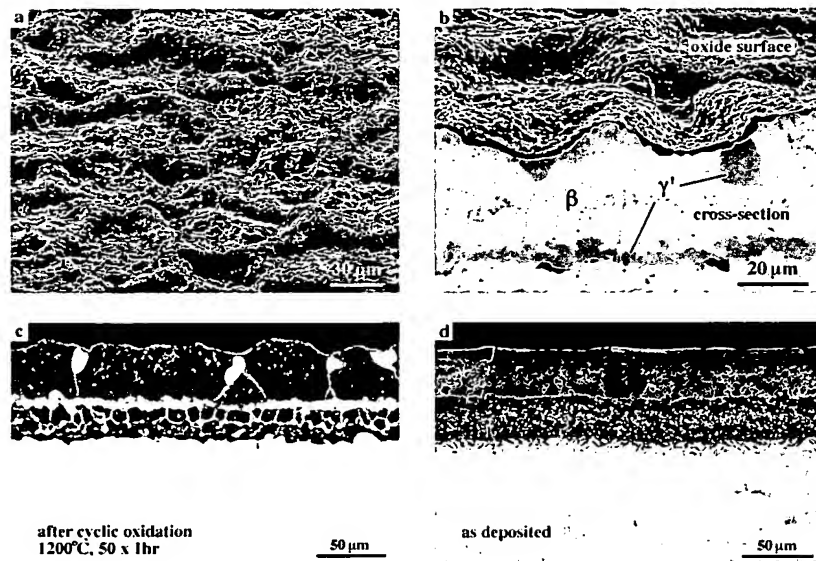


**Figure 10** Microstructure of an initially flat as-aluminized bond coat after 50 1-h cycles at 1200°C: (a) surface rumpling; (b) cross-section showing a rather uniform oxide layer and strong surface undulations ( $\gamma'$ -phase is revealed by etching); (c, d) optical micrographs showing etched cross-section before and after cyclic oxidation. Dark areas on the optical images correspond to the  $\beta$ -phase, whereas the  $\gamma'$ -phase in the coating appears white.

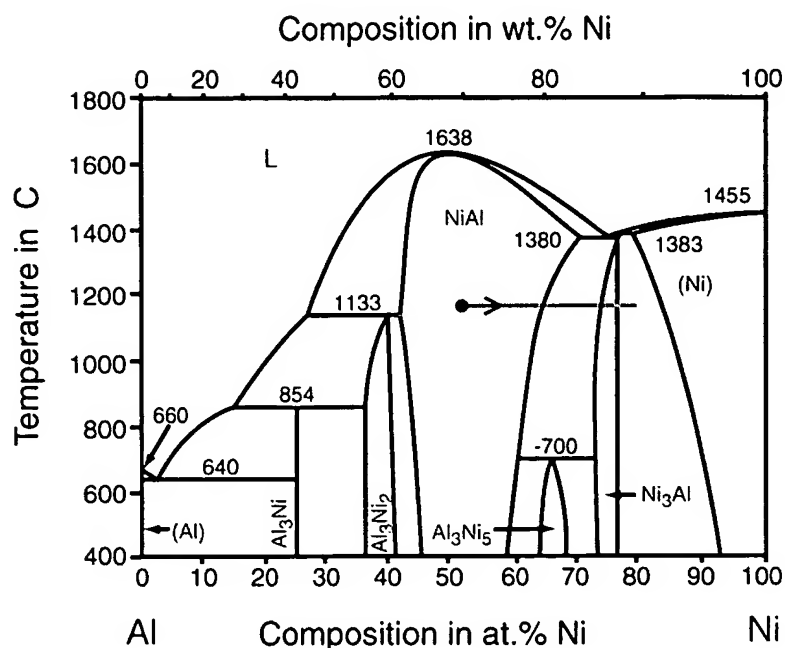


**Figure 11** The Ni-Al pseudo-binary phase diagram illustrating the compositional range of the  $\beta$ -NiAl phase and the direction of the change in composition as the bond-coat is depleted of Al by interdiffusion and selective oxidation.

the single-phase boundary at which point further depletion leads to the formation of  $\gamma'$ -Ni<sub>3</sub>Al. (At even later times, the composition can extend into the  $\gamma$  region of the phase diagram.) Martensitic structures within the  $\beta$ -NiAl phase field also form as the phase boundary is approached. Whereas the martensite start temperature,  $M_S$ , of the pure  $\beta$ -NiAl compositions is known to be generally around room temperature to 300°C (20), the additional Pt, Co, and Cr present in the PtNiAl bond-coat increase the  $M_S$  temperature, and Hemker et al. have reported  $M_S$  temperatures of ~600°C (21).

Substantial progress has been made in the past few years in understanding some of the mechanisms that lead to flaw initiation and growth during use (9, 14, 18, 22). These provide the basis for developing life-prediction models, but nevertheless a number of unanswered questions remain. For instance, the micrographs in Figure 8 were obtained from nominally the same superalloy, with the same bond-coat and the same YSZ coating all made by the same manufacturer in the same process manner. This difference in interface separation and roughening is particularly marked in this figure, but it does suggest that even small, but as yet unidentified, concentrations of dopants can have a large effect on life (23).

Insights gained in the past few years into some of the important processes occurring within the coating during use are summarized in Figure 12. Essentially,

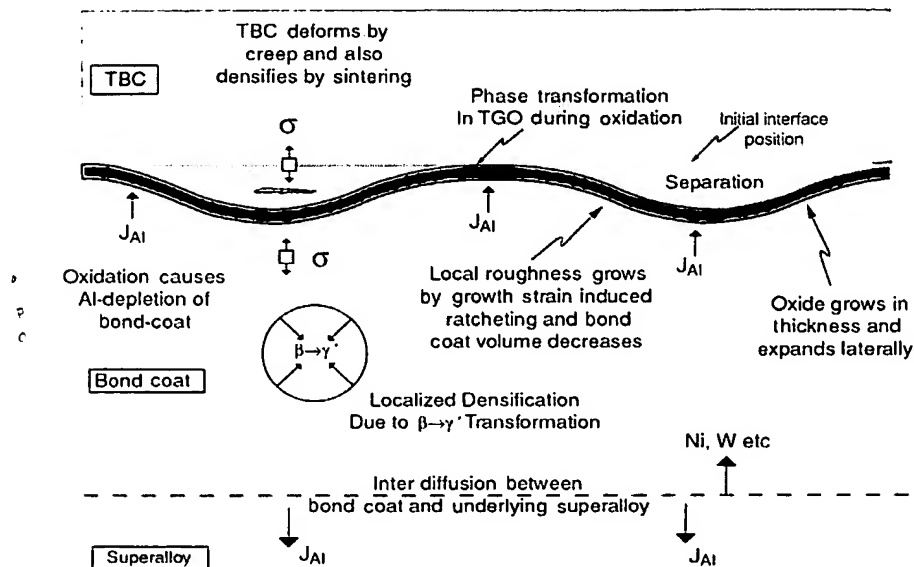


**Figure 12** Schematic summary of the concurrent processes occurring in the bond-coat, TGO and TBC, during use at high temperatures. The complexity in failure times and failure modes is believed to reflect the competition between these individual processes.

the TBC system is one that evolves with time at temperature and its evolution depends in detail on not only the temperature but also on the thermal cycle history and heating and cooling rates, as well as composition.

## NON-DESTRUCTIVE EVALUATION

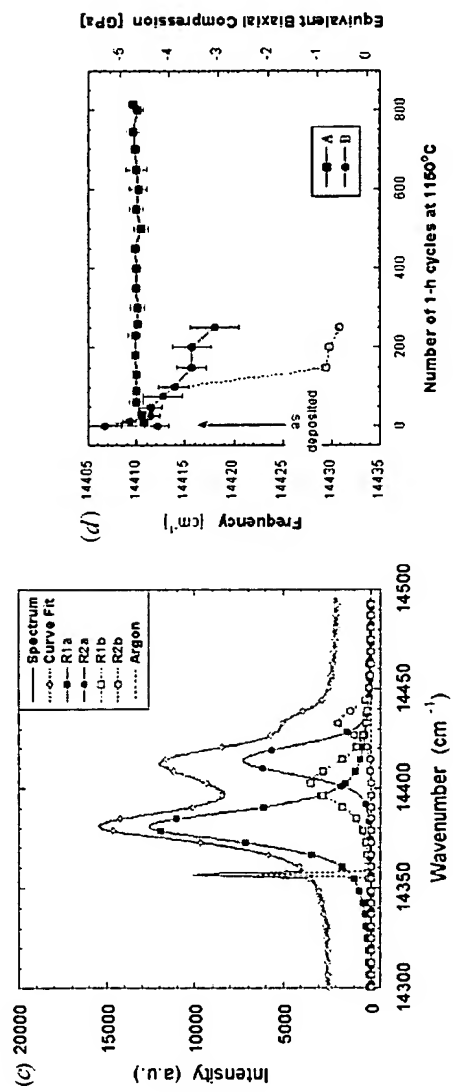
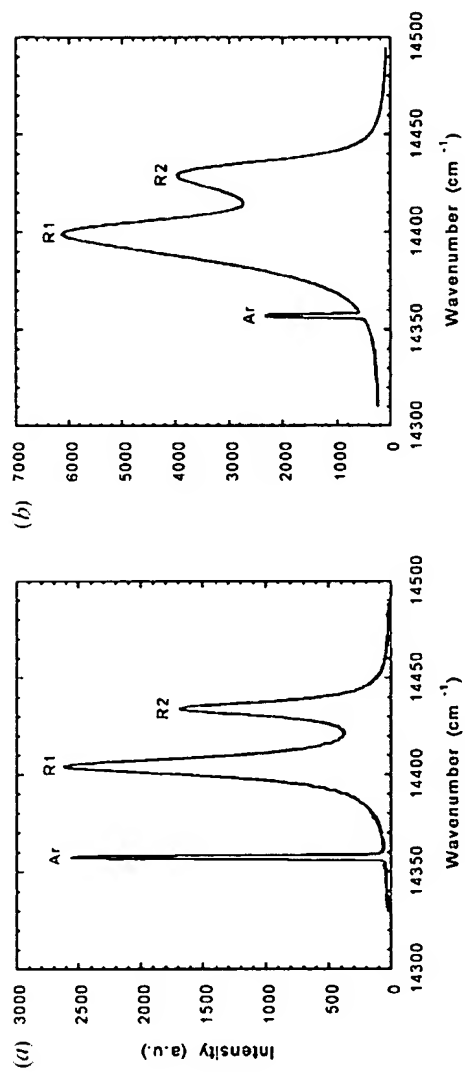
As the design of coatings shifts to a philosophy of prime reliance, the ability to non-destructively monitor the coating, identify defects, and evaluate its remaining life becomes more important. In addition, there is a growing economic pressure to defer maintenance and replacement of parts until really necessary. (The costs are staggering: The cost, in replacement electricity alone, of taking a power generation turbine out of operation can be of the order of \$1 million a day. The cost of replacing a single, first-stage turbine blade can also be very high. Depending on its size the cost can be as high as \$10,000.)

In the case of large area separations, several millimeters to centimeters, infrared imaging provides a direct means of visualizing incipient coating failure provided the blade can be accessed. Usually, though, a coating has failed by the time the separation reaches such a large size, and thus methods of identifying damage at an earlier time, and hence smaller size, are required. No single solution appears practical at this stage, although laser-induced acoustic sounding (from Lasson

Technologies, personal communication) and higher-spatial resolution imaging using polarized scattered light have shown promise in detecting deliberately created interface flaws (25). An alternative method is one that utilizes piezospectroscopy, the strain-induced shift of luminescence and Raman lines. When illuminated with a laser having an appropriate wavelength, luminescence from the aluminum oxide TGO formed by oxidation on the bond-coat can be detected through the thickness of the TBC (26, 27). The luminescence spectrum, from  $\text{Cr}^{3+}$  ions incorporated into the alumina TGO as it grows, is sensitive to the stress state in the TGO. (Because zirconia is a wide band-gap material, it is transparent in the visible so illumination in the blue or green, e.g., as an argon ion laser, can penetrate to the TGO, and the stimulated luminescence, which is in the red, is transmitted back through the coating.) The key to the use of photoluminescence as an NDE tool is that the frequency of the luminescence lines shifts with mean stress and the shape of the luminescence lines is a direct measure of the stress distribution within the region of the TGO probed by the laser. As described in detail elsewhere, the luminescence lines can be deconvoluted and the degree of damage and local interface separation evaluated (11, 15). Since this can be performed using focused lasers and is also nondestructive, piezospectroscopy-based methods show particular promise as a NDE tool for evaluating coatings. An example is illustrated in Figure 13a,b, that is a comparison of spectral data from two coatings. In Figure 13a, there little change in spectral shift with thermal cycling, the TGO remains flat and does not fail within the time of the experiments (*curve A* in Figure 13c) In Figure 13b, a continuous change in frequency (*curve B* in Figure 13c) is shown that exhibited substantial spectral broadening and failed after several hundred cycles, an average value but shorter than the other.

## SINTERING AND DENSIFICATION

One of the concerns in developing a reliable and robust coating is how the coating changes during use at high temperatures. By analogy with the behavior of other porous ceramics, it might be expected that the coating will densify by the reduction in surface energy associated with the excess surface area of the pores. This process is commonly referred to as sintering. There are two principal concerns. One is that densification inevitably increases the elastic modulus and thereby decreases the strain compliance of the coating. The other is that densification decreases the volume fraction of porosity which, in turn, causes the thermal conductivity to increase. Although the kinetics of densification of bulk, free-standing zirconia ceramics is well characterized, evaluation of these effects in actual coatings is not. In part this is because of the peculiar geometry of the porosity in plasma-sprayed and electron-beam deposited coatings. In a bulk ceramic, porosity tends to be spherical in shape, whereas it is plate-like in plasma-sprayed coatings and columnar-like in EB-PVD TBCs. These differences in pore shape and topology are compounded by the fact that the densification of a TBC is constrained by the presence of the underlying alloy, which has not yet been investigated in detail.



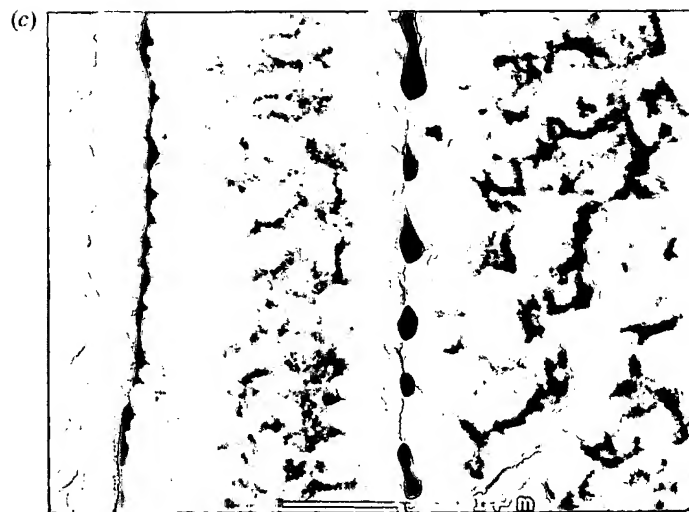
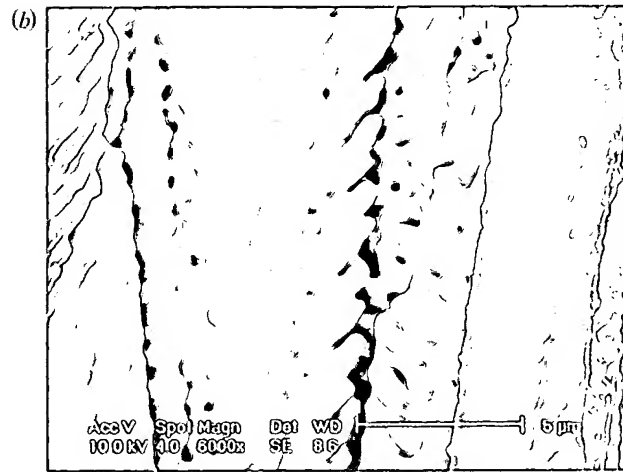
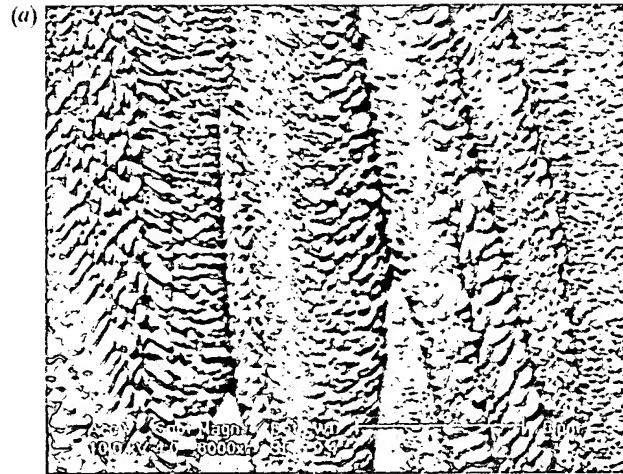
In fact, it is quite likely that the densification of plasma-sprayed and EB-PVD TBCs might be quite different from one another and also from bulk zirconia ceramics on account of the constraint imposed by the alloy. Two possible factors appear to affect densification of coatings. One is the geometric constraint on the lateral shrinkage of the coating by the rigid alloy as the coating tries to densify to lower its overall surface area. This is a classic problem in ceramic sintering known as constrained sintering (28). The other factor is the effect of the stress produced by thermal expansion mismatch between the coating and the alloy. For instance, EB-PVD TBCs are typically deposited at high temperatures, at about the prospective use temperature, whereas the majority of plasma-sprayed coatings are deposited at substantially lower temperatures. As a result, unless extensive strain relaxation can occur in the coating at operating temperatures, the difference in thermal expansion between the alloy and the TBC will produce stresses that can affect densification. In the case of the plasma-sprayed coatings, they will be under a tensile stress during operation that would tend to retard densification. Lack of experimental data on the creep strain relaxation of PSZ coatings and their densification rate presently limits analysis of these factors.

Some insights into the mechanisms of densification have recently been gained from microstructural observations of coatings at different stages in their life. In plasma-sprayed coatings, the initially formed disc-shaped pores, typically formed at the splat boundaries, change shape by spheroidizing in much the same way as interconnected porosity breaks up and spheroidizes during the initial and intermediate stages of sintering packed powders. A different process appears to occur with EB-PVD coatings. Based on micrographs of coating cross-sections and the known differences in thermal expansion coefficient between zirconia and superalloys (Figure 3) it has to be concluded that the majority of the individual columns in a coating will not be in contact at a typical operating temperature. The dilemma is then how densification occurs when there are gaps between the columns and what the mechanism of sintering might be. Examination of micrographs recorded after different times point to a possible sintering mechanism (Figure 14). In their as-deposited state, the columns have a feathery shape due to shadowing effects and the continuing change in incident flux direction during deposition on a rotating sample (29). The short wavelength features of this very rough, feathery surface morphology rapidly smooth out by surface diffusion to create the more undulating

---

**Figure 13** (a) Characteristic R1 and R2 luminescence spectrum recorded through an intact TBC (a), a damaged TBC (b). Deconvolution of spectrum (b) into components characteristic of the evolving damage in the form of interface separation (c). (d) Comparison between the stresses in the TGO, derived from spectral deconvolution, of two different coatings as a function of thermal cycle life. The upper, unchanging data are from a coating that exhibits no damage over a period of 800 h. The other data are from a coating that steadily degrades with thermal cycling.





surface morphology shown in Figure 14*b*. This occurs quite rapidly, typically 30–100 h at temperatures from 1050–1200°C. Cross-sections of the columns produced by fracturing indicate that the diffusional smoothing is restricted to the surface, where a distinct skin appears to have formed, and that internal porosity just below the surface remains such as shown in Figure 15 (V. Lughi & D.R. Clarke, unpublished data). Continuing exposure at high temperature causes perturbations with a positive radius of curvature on the surface to grow in amplitude with time since they have a higher chemical potential than the regions of negative curvature, i.e., in much the same way as a Rayleigh instability grows (31). Concave perturbations growing on facing, adjacent columns impinge and form a neck, Figure 14*c* (V. Lughi & D.R. Clarke, unpublished data). Once formed, the surface tension associated with these necks creates a sintering force drawing the columns together. The net sintering force depends on the surface tension of the coating and geometric effects such as the average number of necks formed along the length of the columns and their average diameter and spacing. The difference from the usual form of sintering in bulk materials is that the column geometry creates a sintering force that is only in the plane of the coating.

Because densification is a thermally activated process, it is likely that coating sintering and densification will become of even greater significance in the design of future coatings for higher temperature usage. The effects will be exacerbated by having coating materials with lower thermal conductivity than today's YSZ materials because the larger thermal gradient across the coating will result in larger gradients in density and hence in strain compliance.

At the present stage in development, other TBC failure mechanisms dominate life, but eventually the reduction in strain compliance produced by sintering and densification at higher use temperatures is likely to control the life of coatings.

## PHASE STABILITY OF YSZ

The majority of TBCs are yttria-stabilized zirconia containing 7–8 mol%  $\text{YO}_{1.5}$ . Under equilibrium conditions, yttria stabilizes a tetragonal phase above about 1050°C as indicated by the pseudo-binary phase diagram in Figure 16 (32, 33). On cooling, the equilibrium tetragonal phase transforms to a mixture of monoclinic and cubic zirconia unless it is mechanically constrained (33). However, because both

←  
**Figure 14** Sequence of micrographs of an EB-PVD coating showing the evolution of the surface of the columns with time at temperature. The initial feathery surface (*a*) produced by the rapid deposition process smooths out (*b*) with surface fluctuations growing and impinging to form necks between adjacent columns (*c*).

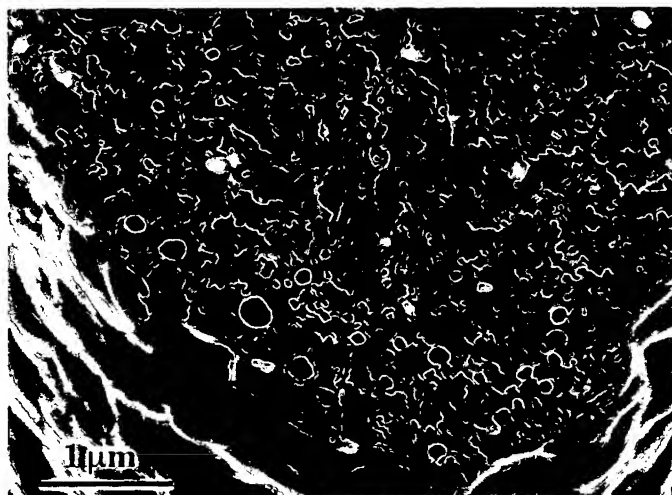


**Figure 15** Fracture through a column of a coating deposited by EB-PVD illustrating the smooth surface region and isolated pores within the columns.

plasma-spraying and electron-beam deposition are high-rate,<sup>3</sup> nonequilibrium processes, the majority of TBCs have the closely related tetragonal-prime structure, a metastable phase, rather than the tetragonal structure. This is of crucial importance because the transformation of tetragonal zirconia to monoclinic invariably causes cracking and failure, clearly undesirable in a coating, whereas the tetragonal-prime does not transform. Indeed, early work by Stecura (34), since reconfirmed several times, demonstrated that coatings having the tetragonal-prime structure exhibited the longest life under thermal cycling. Although strictly metastable, the tetragonal-prime phase, which is sometimes referred to as a non-transformable tetragonal phase, has been found to be stable for prolonged periods of time at high temperature, at least 350 h at 1400°C (V. Lughi & D.R. Clarke, unpublished data). The transformation of the tetragonal-prime phase to a mixture of tetragonal and cubic phases requires diffusion of Y and its spatial partitioning to create regions of tetragonal and cubic phases, and so the long-term stability of the tetragonal-prime is believed to be a direct consequence of both slow diffusion of Y in zirconia and a small driving force (35).

According to nonequilibrium thermodynamic arguments, the regime of temperature and composition over which a metastable structure, such as the tetragonal-prime phase, can exist are bounded by the  $T_o$  lines. These lines, indicated by the dotted lines in Figure 16, are calculated from the free energy functions describing

<sup>3</sup>High-rate compared with vapor-deposition methods, such as molecular beam epitaxy (MBE), used in electronic materials fabrication, for instance.

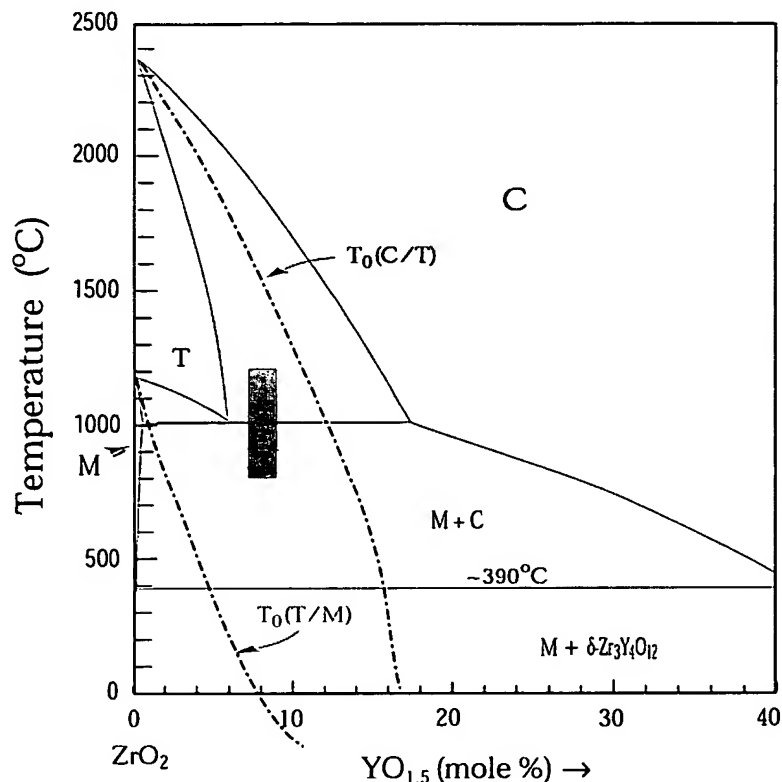


**Figure 16** The zirconia-rich corner of the  $\text{ZrO}_2$ - $\text{YO}_{1.5}$  binary phase diagram. Existing YSZ coatings have a composition and operate over a temperature range shown by the *hatched* region. The tetragonal-prime phase is meta-stable within the  $T_o$  bounds shown as *dashed lines* superimposed on the phase diagram.

the individual phases. The position of the  $T_o^{t/m}$  line shown in the figure has been confirmed through cyclic heating experiments on electron-beam deposited TBCs having different compositions (36). The practical importance of the  $T_o$  lines is that they represent limits to the long-term stability of the tetragonal-prime structure and so can be used to define the maximum range of stabilizer and operating temperatures over which the structure is likely to persist. For instance, it might be tempting to increase the operating temperature by decreasing the yttria content below 8 mol%  $\text{YO}_{1.5}$  since the tetragonal phase field extends to higher temperatures as the yttria content is decreased. However, in doing so, the  $T_o^{t/m}$  line would be crossed on cooling leading to the formation of monoclinic and consequent failure.

As the high temperature stability and thermal conductivity are limited by the stability range of the tetragonal-prime zirconia, there has been growing interest in the use of both alternative stabilizers and the use of co-stabilization by adding

another stabilizer to yttria. Although there was some investigation of alternate stabilizers in the early days of the development of TBCs, lately there has been renewed interest in exploring these alternatives. Much of the motivation has been in using rare-earth stabilizers to decrease the attainable thermal conductivity (see below). In contrast to the development of YSZ, where much of the phase stability had already been determined, little is known about the compositional range of stability of tetragonal and cubic zirconia with different dopants. Indeed, there is growing evidence that there are errors in some of the binary phase diagrams of zirconia with alternate rare-earth stabilizers. Investigation of the phase stability of zirconia with two co-dopants is now underway, and the results of one such study are reproduced in Figure 17, *top* (37). The diagram presents the regions of stability of different phases in the  $\text{ZrO}_2\text{-GdO}_{1.5}\text{-YO}_{1.5}$  system, including the  $\text{Gd}_2\text{Zr}_2\text{O}_7$  pyrochlore phase that has recently been found to have a lower thermal conductivity than 7 YSZ. In Figure 17, *bottom*, details of the stability region for the tetragonal-prime phase are shown, clearly demonstrating that although gadolina ( $\text{GdO}_{1.5}$ ) is effective in stabilizing tetragonal and cubic zirconia, the stability range of the tetragonal-prime phase is more restricted than for the case with yttria. Only with the completion of such comprehensive, but time-consuming, studies will there be a firm thermodynamic basis for understanding the high-temperature stability of alternative coatings.

One of the striking findings to have come from numerous studies around the world is that coatings having the 7–8 mol%  $\text{YO}_{1.5}$  composition exhibit the longest thermal cycle life. Both small increases in the yttria concentration and coatings based on alternative stabilizers and co-stabilized coatings all fail at significantly smaller number of thermal cycles, whether they are deposited by electron beam evaporation or by plasma-spraying (38). The reason why the 7–8 mol%  $\text{YO}_{1.5}$  composition is special remains one of the major unresolved questions in the field. It has been noted, correctly, that zirconia ceramics, such as the partially stabilized zirconias, having similar yttria contents, have unusually high fracture toughness (33). This is a result of transformation toughening, which is the increase in toughness associated with the phase transformation from tetragonal to monoclinic structure. However, since these coatings do not undergo the transformation, the toughening mechanism cannot operate and the exceptional thermal cycle life cannot be the result of the material having a high fracture toughness from transformation toughening.

## APPROACHES TO DECREASING THERMAL TRANSPORT

As future engine designs call for higher gas temperatures, the importance of a coating that minimizes both thermal conductivity and radiative heat transfer from the gas to the underlying superalloy also increases. (It is unlikely that the outer temperature of the metallic bond-coat or superalloy can be raised.) Despite the fact that YSZ is transparent in the infrared, radiative heat transfer through the YSZ coating is only a minor contribution at present gas temperatures because of optical scattering within the coatings (Figure 18) (39). However, as the radiative power of

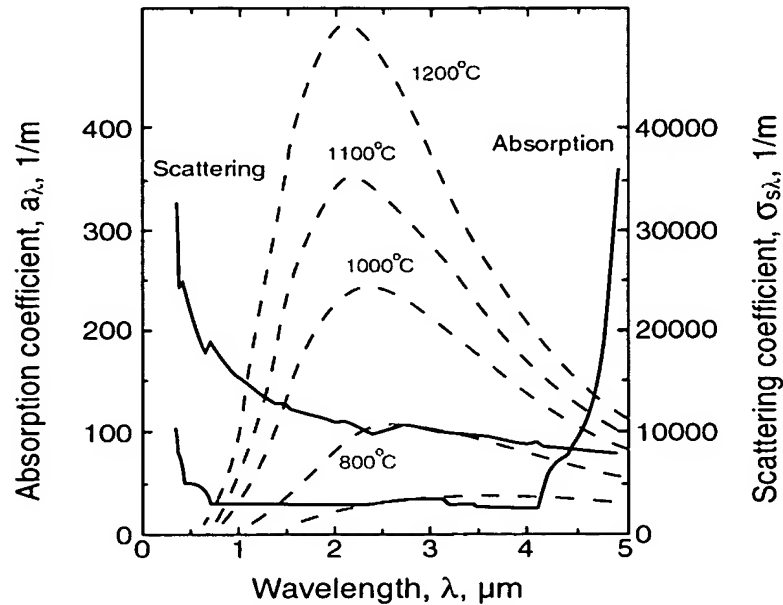


**Figure 18** The optical absorption and scattering coefficients for YSZ zirconia. Superimposed are the black-body radiation curves for a number of temperatures indicating that yttria-stabilized zirconia is, apart from scattering, transparent to radiative transport at the wavelengths pertinent to a combustion environment; redrawn from (39).

a hot gas, assuming it radiates as a black-body, increases with the fourth-power of its temperature, radiative heat transfer through the coating is expected to become a concern in the design of future coatings.

The most effective means of reducing radiative heat transfer would be to have a reflective layer on the outer surface of the coating. At present it is not known how to create such a reflective layer that will also withstand the long-term erosion that occurs from small particulates flowing through the engine. An alternative approach would be to fabricate a multilayer coating whose combination of layer thickness and optical properties lead to increased reflectivity in the infrared. Although this is, in principle, a viable approach, and is commonly used, for instance, in forming Bragg mirrors for vertical cavity semiconductor lasers (VCSELs), it calls for very stringent requirements for the flatness of the individual layers to have any appreciable reflective efficiency (40). For instance, for multilayers of YSZ and alumina,<sup>4</sup> a system that has been fabricated, the interface roughness must be less than 5 nm. Also, a multiple stack of multilayers, each with a different period, would be needed to reflect any appreciable fraction of the broad band infrared radiation from the hot gas. In addition to the practical difficulties involved in making multilayers with the

<sup>4</sup>This multilayer system, deposited by sputtering, is currently used as an anti-counterfeiting device in high-denomination Canadian bank notes.

required interfacial smoothness, the layers would be susceptible to break-up and spheroidization (analogous to Rayleigh instability) driven by reduction in overall interfacial energy, with consequent reduction in reflective efficiency. Evidence for such multilayer break-up has been reported in YSZ/alumina-multilayered TBCs (41).

As an alternative to creating a reflective coating, attempts have also been made to reduce radiative transport by incorporating infrared absorbers that convert the infrared to lower energy phonons. To make the most of the thermal resistance of the coating, these would, ideally, be placed in the outer regions of the coating. The most straightforward is to incorporate a second phase, such as NiO, that is highly absorbing in the infrared. Attempts to do so, however, have led to increases in thermal conductivity and increased rate of sintering. A second absorbing strategy is to incorporate dopant ions into the coating that have broad absorption bands in the infrared and re-emit at longer wavelengths. It has been suggested that many rare-earth ions would fulfill this requirement, especially as many of them are also soluble in YSZ and can serve as stabilizers. A potential drawback, though, is that they may decrease the high-temperature phase stability of the tetragonal-prime YSZ. Further phase equilibria studies will need to be carried out to evaluate this problem.

The search for oxide materials having a lower thermal conductivity than YSZ zirconia has, in many respects, just begun. The study of thermal conductivity at very high temperatures has been a largely neglected field since the work of Kingery and colleagues in the 1950s (Figure 19a) (42). They measured the thermal conductivity of many oxides as a function of temperature, studied the effects of porosity and the effects of mixing two different oxides. They also demonstrated that the thermal conductivity of almost all oxides decreased as  $1/T$  in accord with the thermal conductivity being controlled by the Umklapp inelastic phonon-phonon scattering process.<sup>5</sup> The majority of their measurements did not extend to the temperatures of interest for future TBCs, but they did find that three oxides, YSZ,  $\text{UO}_{2-x}$ , and  $\text{Th}_{0.7}\text{U}_{0.3}\text{O}_{2+x}$  exhibited a temperature-independent thermal conductivity at high temperatures, quite different from the other crystalline oxides but very similar to that of fused silica<sup>6</sup> (Figure 19a). The absence of the characteristic  $1/T$  dependence was ascribed to the fact that both YSZ and  $\text{UO}_{2-x}$  contain a very high concentration of point defects and that the defects cause phonon scattering. An estimate of the point defect spacing can be made based on the fact that an oxygen vacancy is introduced into the zirconia structure for every two  $\text{Y}^{3+}$  that substitutes for two  $\text{Zr}^{4+}$  ions. For 8 m/o YSZ, the average distance between oxygen vacancies is only  $\sim 1$  nm. Similarly, the low, temperature-independent thermal conductivity of fused silica and other glasses has been attributed to their random structure, precluding

<sup>5</sup>After correction for the temperature dependence of the thermal expansion.

<sup>6</sup>Interestingly, monoclinic zirconia, which does not contain any stabilizers and hence no associated structural point defects, exhibits the classical  $1/T$  dependence due to Umklapp scattering (Figure 20a).

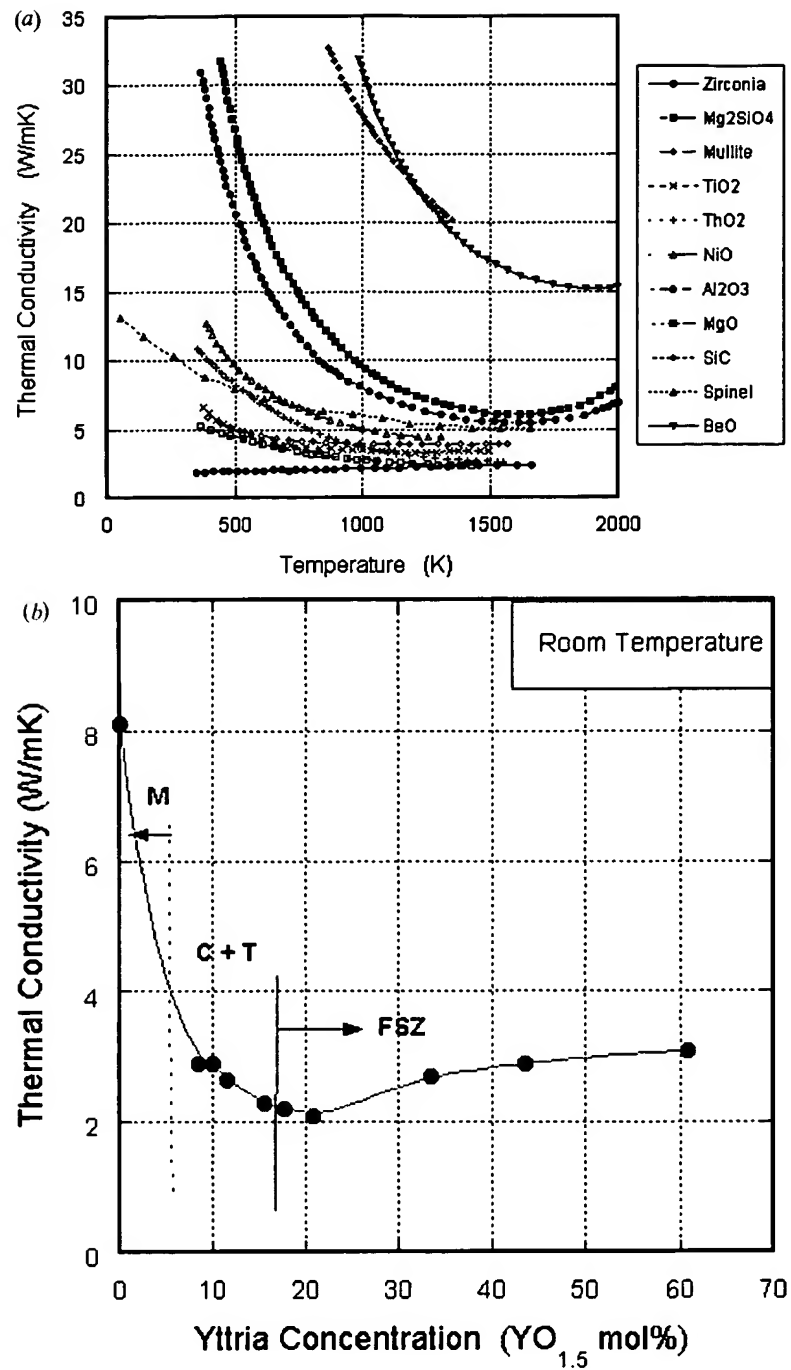


**Figure 19** (a) Thermal conductivity of a number of oxide ceramics, after Kingery (42). (b) Thermal conductivity of yttria-stabilized zirconia as a function of yttria content, after Bisson et al. (66).



any long wavelength phonon modes with the dominant phonon contributions being limited by the tetrahedral unit of the glass (43). Because grain boundary scattering is an extrinsic mechanism limiting thermal conductivity, a number of investigators have advocated using nanocrystalline materials to decrease the thermal conductivity. While this may well prove to be an effective strategy for other ceramics, measurements on nanocrystalline-stabilized zirconia indicate that it is not because the thermal conductivity is unaffected by grain size, even down to a grain size of 65 nm (44) (Figure 20a). The most likely explanation is that the mean free path of the point defects in YSZ is significantly smaller than even the smallest grain size attainable in nanocrystalline YSZ.

For many years it was considered that the high-temperature conductivity of silica glass represented the lower limit—the so-called amorphous limit—to the thermal conductivity of materials at high temperatures. By extension, it seems to have been assumed that there was little likelihood of discovering oxides with a lower thermal conductivity than YSZ. However, recent discoveries that related compounds, such as  $\text{Gd}_2\text{Zr}_2\text{O}_7$ ,  $\text{La}_2\text{Zr}_2\text{O}_7$ , and  $\text{Sm}_2\text{Zr}_2\text{O}_7$ , all have lower thermal conductivity than YSZ (45,46) have stimulated a fresh search (Figure 20b). Interestingly, none of these zirconate compounds, which have the pyrochlore crystal structure, have structural vacancies so there remains some uncertainty as to the reason for the low thermal conductivity of these materials. Furthermore, there is no reported difference in the thermal conductivity between the ordered and disordered forms of the  $\text{Gd}_2\text{Zr}_2\text{O}_7$  phase. Recently, an oxide,  $\text{W}_3\text{Nb}_{14}\text{O}_{44}$ , belonging to yet a different class of oxides, the substituted  $\text{ReO}_3$ , has been shown to have comparable and temperature-independent thermal conductivity (47).

Theory presently provides little guidance in selecting candidate materials that will exhibit low thermal conductivity at high temperatures. The Umklapp scattering process provides a ready explanation for the  $1/T$  dependence, but the thermal conductivity cannot continue to decrease in this manner indefinitely. Indeed, once the phonon-scattering length and wavelength fall much below the inter-atomic spacing, the thermal conductivity is expected to become temperature independent and plateau out at a fixed value. The temperature at which this can be expected to occur is when the dominant phonon wavelength is equal to the inter-atomic distance. Unfortunately, the majority of experimental measurements reported on oxides do not go to a sufficiently high temperature for this limiting behavior to be observed except for those shown in Figure 19a. By invoking the concept that this limiting thermal conductivity can be computed from the condition that the dominant phonon wavelength is equal to the inter-atomic spacing, the limiting thermal conductivity can be expressed as

$$\kappa_{\min} \rightarrow 0.87k_B N_A^{2/3} \frac{m^{2/3} \rho^{1/6} E^{1/2}}{M^{2/3}}, \quad 2.$$

where  $M$  is the molecular weight,  $m$  is the number of atoms per molecule,  $\rho$  is the density of the crystal structure,  $E$  is Young's modulus, and  $k_B$  and  $N_A$  are Boltzmann's constant and Avogadro's number (48). This expression is expected to be a lower

estimate for the plateau conductivity because it does not account for contributions to the conductivity from optical phonon modes. Nevertheless, in the absence of any alternatives, it provides a means of selecting potential materials for experimental screening.

An alternative strategy in finding materials that exhibit low thermal conductivity would be the use of combinatorial approaches, such as those that have already met with some success in identifying new phosphors and ferroelectrics. Despite its obvious attraction in screening multicomponent oxides, no progress has been made in this area because of the lack of a rapid method of measuring thermal conductivity. Even with the standard thermal flash technique, measurements at a single temperature can typically take tens of minutes each.

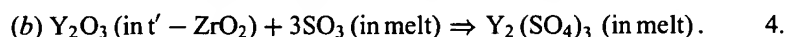
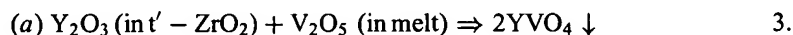
In the absence of a generally accepted model for high-temperature thermal conductivity, several groups have attempted to decrease the thermal conductivity of zirconia by altering the concentration of stabilizer, using alternative rare-earth stabilizers and mixing them (49–51). The rationale for many of these investigations is that the thermal conductivity, at least within the  $1/T$  regime, is sensitive to the differences in atomic mass and ionic size. Seminal studies of this type, below the Debye temperature, were conducted in the 1960s substituting Ge for Si in Si-Ge alloys and substituting In into GaAs (52, 53). Some of the recent investigations appear to have also been guided by the fact that additions of aliovalent dopants introduce point defects into the crystal structure. This effect is clearly seen in the yttria-zirconia system because there is almost no difference in atomic mass between Y and Zr and the principal effect of increasing yttria concentration is to increase the concentration of oxygen vacancies (Figure 19b). Since the majority of thermal conductivity measurements reported have been on coatings as distinct from fully dense materials, it has not yet been possible to distinguish between the effects of the stabilizing dopants and changes in density produced by the different stabilizer. Once more systematic studies of dense materials, including measurements made at high temperatures, in excess of  $1000^{\circ}\text{C}$ , have been made, a clearer idea of the factors that determine thermal conductivity will be gained and models can then be constructed.

Finally, of course, the traditional method of reducing thermal conductivity of a solid is to incorporate porosity (54, 55). The porosity decreases thermal conductivity by effectively decreasing the section of material through which heat flows. In fact, all present TBCs, whether deposited by plasma-spraying or by electron beam evaporation, contain porosity by design. The porosity has two functions, one is to increase the strain compliance of the coating and the other is to decrease the thermal conductivity. The porosity of plasma-sprayed coatings is generally associated with splat boundaries and consequently is disk-shaped parallel to the coating. Such a shape is particularly effective in minimizing heat transport through the coating, and as-deposited plasma-sprayed coatings can have a thermal conductivity as low as 50% of fully dense YSZ. The dominant form of porosity in EB-PVD coatings is the gaps between columns. As these are oriented perpendicular to the coating, the reduction in thermal conductivity is less marked but nevertheless can be as high as 30% in an as-deposited coating. The problem with this extrinsic form of

thermal conductivity reduction is that pores coarsen, and as the coatings sinter, the volume fraction of porosity decreases. Because both coarsening and sintering are thermally activated processes, a method of stabilizing porosity is needed in order for porosity to remain an effective contribution to thermal conductivity reduction at higher temperatures than is found in today's coatings.

## CORROSION

Hot corrosion in gas turbines has been a longstanding concern (56), surfacing prominently in the context of military aircraft operation over seawater (57). The problem results from the ingestion, from the environment, of salt that combines with S and V impurities in the fuel to yield highly corrosive mixtures of sodium sulfates and vanadates with relatively low melting points. When these mixtures deposit on a conventional YSZ thermal barrier, they can lead to the following two reactions (58):



In principle, both reactions induce destabilization of  $t'$  by leaching of Y and shifting its composition toward the range in which it becomes transformable to monoclinic. However, reaction (a) is of greater concern because reaction (b) requires a relatively high partial pressure of  $\text{SO}_3$ , making YSZ much less sensitive to sulfate attack (59, 60). It is also reported that the equivalent reactions with  $\text{ZrO}_2$  are not significant (61).

Among the alternate TBC compositions investigated,  $\text{Sc}_2\text{O}_3$  has also been reported to be more resistant than  $\text{Y}_2\text{O}_3$  to vanadate attack when dissolved in  $t'$  (61), an effect ascribed to its lower activity in solid solution. Much less is known experimentally about the susceptibility of rare-earth oxide stabilizers to reaction, but a cursory examination of the formation energies of RE vanadates (Figure 21) suggests a well-behaved trend with ionic size. [Interestingly, Sc and In, both claimed to be less reactive than Y (62), qualitatively fit this trend.] One would then anticipate that Gd, Sm, and La should be more reactive than Y, although their relative activities in the  $t'$  or zirconate phases may change their relative susceptibilities to this form of attack.

To date, corrosion considerations have received only limited attention in the development of advanced TBCs. Partly this is because of the predominance of clean fuels in current operation of both aerospace and power generation turbines. There are two exceptions. One is CMAS attack, which is perceived to be largely physical in nature, controlled by the wetting characteristics of the coating and thus not expected to vary dramatically within the present menu of viable materials. The other is vanadate corrosion, which is relevant in engines that experience large variability in the quality of available fuels, particularly oil-based rather than natural

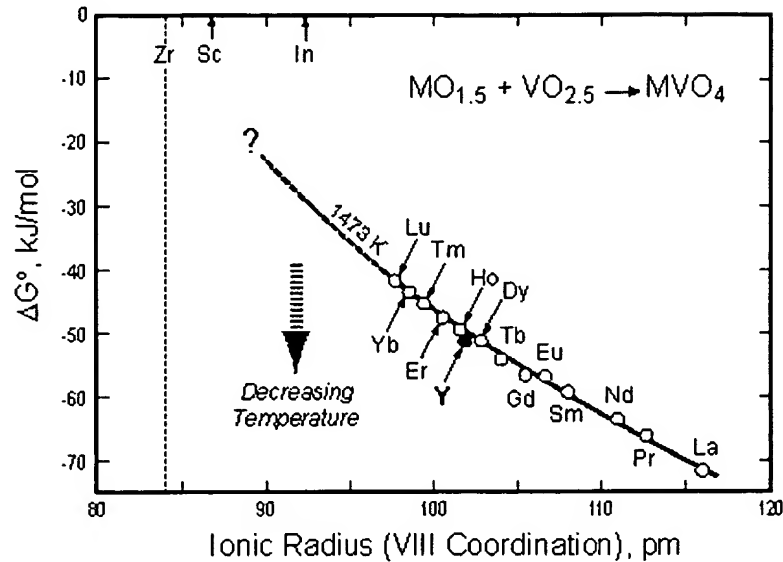


**Figure 21** Free energies of formation,  $\Delta G^\circ$ , of rare-earth vanadates (from oxides) at 1200°C as a function of the rare-earth ionic size (74). Note that decreasing temperature reduces the stability of the vanadate.

gas or jet fueled. There is also the perception that the problem is not relevant once the temperature exceeds the condensation point of the corroding salts ( $\sim 950^\circ\text{C}$ ), but even in high-performance engines there are likely to be colder surfaces that would become susceptible to hot corrosion.

## MATERIALS DESIGN OF FUTURE THERMAL BARRIER COATINGS

Experience with current TBC systems provides a number of directions for the materials selection and design of future coatings. Having to operate at higher temperatures, the kinetics of microstructural evolution of coatings as well as the system dynamics will become even more important than they are today. Although there is some prospect of having a no-bond-coat system by appropriately surface alloying the superalloy components prior to TBC deposition, it is likely that the performance of TBCs will remain limited by the distortions of the bond-coat that develop during exposure and thermal cycling. There is a clear need for an interdiffusion barrier layer between the bond-coat and the superalloy to limit the inward diffusion of aluminum from the bond-coat into the superalloy and the outward diffusion of nickel and other elements, such as W, Ta, into the bond-coat and to the bond-coat/oxide interface.

There is also increasing evidence that when the bond-coat/TGO morphological instabilities on thermal cycling are suppressed, the life of a coating becomes limited by the thickness of the thermally grown oxide. The idea that failure will occur when the thermally grown oxide reaches a critical thickness has been current in the industrial community for several years. Whereas the critical thickness as a fracture mechanics criterion has been developed to describe failure of films stressed by a variety of mechanisms, ranging from lattice coherency to thermal expansion mismatch, the pertinent parameters to describe the failure of TBCs have yet to be fully developed and quantified. Nevertheless, the idea that there may be a maximum critical thickness has motivated TBC processing and the choice of bond-coat alloys that minimize the thickening rate of the TGO on oxidation. Thus impurities introduced during the preparation of PtNiAl bond-coats prior to EB deposition have been found to enhance the growth rate of the TGO (V.K. Tolpygo, submitted). Similarly, maximizing the grain size of the TGO is important to minimize its thickening rate.

At this stage, with the recent focus on developing coatings with lower thermal conductivity than that of YSZ, it is difficult to anticipate which material, if any, will replace YSZ in future coating systems. Co-stabilized YSZ, simultaneously

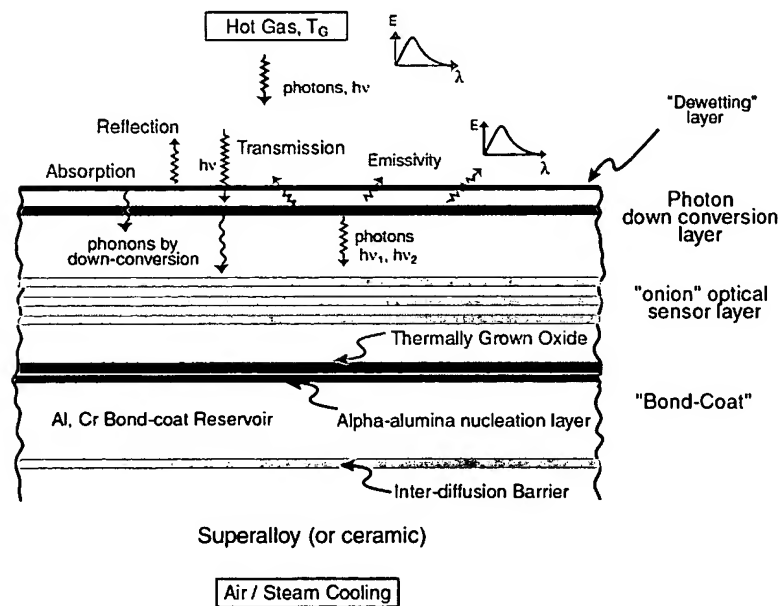


**Figure 22** Schematic illustration of a possible future multifunctional TBC embodying many of the features designed to maximize life at elevated temperatures, reduce radiative heat transport, and provide some sensor capabilities. Not discussed in the text but shown in the figure is an outer layer to alter the wetting behavior of potential corrodants, such as molten CMAS and vanadates.

doped with several different rare-earth ions, has been shown to have significantly lower thermal conductivity than 7YSZ (49). However, although it is believed that they are thermodynamically compatible with an alumina TGO, all the co-stabilized coatings made to date, whether by EB or PS, have exhibited thermal cycle lives inferior to that of 7YSZ. The reason why 7YSZ has the longest life of all the alternative rare-earth doping concentrations remains unresolved and will clearly be the focus of much research in years to come. The pyrochlore zirconates, such as  $\text{Gd}_2\text{Zr}_2\text{O}_7$  and  $\text{Sm}_2\text{Zr}_2\text{O}_7$ , also have lower thermal conductivity than YSZ and have the additional advantage that they too can be deposited by both existing EB and PS technologies. However, they are thermodynamically incompatible with alumina and so probably must be used with an intervening YSZ layer to prevent long-term destabilization.

Whichever material is selected for use as the thermally insulating phase in future TBC systems, it is likely that it will also have to embody some form of capability for use as an embedded sensor. Although an operating turbine and combustor are exceedingly aggressive environments, some form of sensing, even rather rudimentary, is highly desirable. A number of ideas have been proposed based on introducing dopant ions that will fluoresce when illuminated. For instance, it has been proposed to measure the coating temperature by introducing a minor concentration of a rare-earth into YSZ and use the luminescence lifetime as an in situ measurement of temperature (64). Another idea is to make a coating of layers with a different luminescent ion in each and monitor the wear of the coating by monitoring the changes in luminescence as successive layers are eroded away (D.R. Clarke & M. Gentleman, in preparation). Fortunately, such doping approaches are compatible with the strategies being explored in making co-stabilized YSZ coatings and are also compatible with the crystal chemistry of the pyrochlore zirconates. When combined with a need to minimize radiative heat transfer, it is likely that the present monolithic YSZ coating will be replaced by a highly structured coating having the form shown in Figure 22.

The *Annual Review of Materials Research* is online at  
<http://matsci.annualreviews.org>

#### LITERATURE CITED

1. Sims CT, Stoloff NS, Hagel WC. 1987. *Superalloys II*. New York: Wiley
2. Meier GH, Petit FS. 1992. *Mater. Sci. Eng. A* 153:548
3. Kofstad P. 1988. *High Temperature Corrosion*. Amsterdam: Elsevier
4. Miller RA. 1984. *J. Am. Ceram. Soc.* 67:517–21
5. Hindam H, Whittle DP. 1982. *Oxide Metals* 18:245
6. Mutasim Z, Rimlinger C, Brentnall W. 1997. *Am. Soc. Mech. Eng.* GT-531:1–10
7. Tolpygo UK, Clarke DR. In preparation
8. Sergo V, Clarke DR. 1998. *J. Am. Ceram. Soc.* 81:3237–42
9. Evans AG, Mumm DR, Hutchinson JW, Meier GH, Petit FS. 2001. *Prog. Mater. Sci.* 46:505–53
10. Hutchinson JW, Suo Z. 1992. *Adv. Appl. Mech.* 29:63–191

11. Peng W, Clarke DR. 2000. *J. Am. Ceram. Soc.* 83:1165–70
12. Hutchinson JW, He MY, Evans AG. 2000. *J. Mech. Phys. Solids* 48:709–34
13. Tolpygo UK, Clarke DR. In preparation
14. Tolpygo VK, Clarke DR. 2000. *Acta Mater.* 48:3283–93
15. Nychka J, Clarke DR. 2002. *Surf. Coat. Technol.* 146–147:110–16
16. Lipkin DM, Clarke DR. 1996. *Oxide Metals* 45:267–80
17. Clarke DR. 2002. *Curr. Opin. Solid State Mater. Sci.* 6:237–44
18. Karlson AM, Hutchinson JW, Evans AG. 2002. *J. Mech. Phys. Solids* 50:1565–89
19. Choi SR, Hutchinson JW, Evans AG. 1999. *Mech. Mater.* 31:431–37
20. Smialek JL, Hehemann RF. 1973. *Met. Trans.* 4:1571–75
21. Chen MW, Ott RT, Hufnagel TC, Wright PK, Hemker KJ. 2003. *Surf. Coat. Technol.* 163:25
22. Tolpygo VK, Clarke DR, Murphy KS. 2001. *Surf. Coat. Technol.* 146:124–31
23. Tolpygo VK, Murphy KS, Clarke DR. 2001. *Met. Mater. Trans.* 32A:1467
24. Deleted in proof
25. Tolpygo VK, Clarke DR. 2003. *Surf. Coat. Technol.* 163–164:81–86
26. Clarke DR, Murphy KS, Paton N. 2000. *U.S. Patent No. 6,072,568*
27. Christensen R, Lipkin DM, Clarke DR, Murphy KS. 1996. *Appl. Phys. Lett.* 69:3755–58
28. Bordia RK, Jagota A. 1993. *J. Am. Ceram. Soc.* 76:2475
29. Terry SG, Litty J, Levi C. 1999. In *Elevated Temperature Coatings: Science and Technology III*, ed. J Hampkian, NB Dahotre, pp. 13–25. Warrendale, PA: Min. Met. Mater. Soc.
30. Deleted in proof
31. Nichols FA, Mullins WW. 1965. *J. Appl. Phys.* 36:1826
32. Du Y, Jin Z, Huang P. 1991. *J. Am. Ceram. Soc.* 74:1569–77
33. Green DJ, Hannink RHJ, Swain MV. 1989. *Transformation Toughening of Ceramics*, Boca Raton, FL: CRC Press
34. Stecura S. 1985. *NASA Tech. Bull.* 86905
35. Rebollo NR, Fabrichnaya O, Levi C. 2003. *Z. Metall.* In press
36. Lugh V, Tolpygo VK, Clarke DR. 2003. *J. Am. Ceram. Soc.* 94:163–70
37. Leckie RMR, Rebollo NR, Yang JC, Levi C. 2003. *Surf. Coat. Technol.* In press
38. Zhu D, Nesbitt JA, McCue TR, Barrett CA, Miller RA. 2002. *Ceram. Eng. Sci. Proc.* p. 23
39. Siegel R, Spuckler CM. 1998. *Mater. Sci. Eng. A* 245:150–59
40. Coldren LA, Corzine SW. 1997. *Laser Diodes and Integrated Photonic Circuits*. New York: Wiley & Sons
41. Fritscher WK, Schulz U, Leyens C, Peters M. 1999. *Int. Symp. Ceramic Materials and Components for Engines*. Goslar, Germany
42. Kingery WD. 1955. *J. Am. Ceram. Soc.* 38:251–56
43. Kittel C. 1949. *Phys. Rev.* 75:972
44. Raghavan S, Wang H, Dinwiddie RB, Porter WD, Mayo MJ. 1998. *Scripta Mater.* 39:1119–25
45. Maloney MJ. 2000. *U.S. Patent No. 6,117,560*
46. Vassen R, Cao X, Tietz F, Basu D, Stover D. 2000. *J. Am. Ceram. Soc.* 83:2023–28
47. Winter M, Cheetham A, Clarke DR. 2003. *J. Am. Ceram. Soc.* Submitted
48. Clarke DR. 2003. *Surf. Coat. Technol.* 163–164:67–74
49. Zhu D, Miller RA. 2002. *Ceram. Eng. Sci. Proc.* 23:457–68
50. Leclercq B, Mevrel R, Liedtke V, Hohenauer W. 2003. *2nd. Int. Meet. Space and Aerospace Materials Technology*, Siebrsdorf, Germany. In press
51. Clarke DR, Murphy KS. 2001. *U.S. Patent Application*. Pending
52. Abeles B, Beers DS, Cody GD, Dismukes JP. 1962. *Phys. Rev.* 125:44
53. Abrahams MS, Braunstein R, Rosi FD. 1959. *Phys. Rev.* 10:204

54. Kingery WD, Bowen HK, Uhlmann DR. 1976. *Introduction to Ceramics*. New York: Wiley & Sons
55. Lu TJ, Levi C, Wadley HNG, Evans AG. 2001. *J. Am. Ceram. Soc.* 84:2937–46
56. Goebel JA, Pettit FS. 1970. *Metall. Trans.* 1:1943
57. Rapp RA. 2002. *Corrosion Sci.* 44:209–21
58. Jones RL. 1991. *Mater. High Temp.* 9: 228–36
59. Jones RL. 1996. In *Thermal Barrier Coatings in Metallurgical and Ceramic Protective Coatings*, ed. KH Stern, pp. 194–235. London: Chapman & Hall
60. Marple BR, Voyer J, Moreau C, Nagy DR. 2000. *Mater. High Temp.* 17:397–412
61. Jones RL. 1996. *Naval Res. Lab. Rep.* Washington DC
62. Jones RL, Mess D. 1992. *J. Am. Ceram. Soc.* 75:1818–21
63. Deleted in proof
64. Feist JP, Heyes AL, Choy KL, Mei J, Nicholls JR. 2001. *Proc. Inst. Mech. Eng.* 215:333–35
65. Deleted in proof
66. Bisson J-F, Fournier D, Poulain M, Lavigne O, Mevrel R. 2000. *J. Am. Ceram. Soc.* 83:1993
67. Wray KL, Connolly TJ. 1959. *Appl. Phys.* 30:1702
68. Lee WD, Kingery WD. 1960. *J. Am. Ceram. Soc.* 43:594
69. Simpson J. 1962. *Boeing Comp. Rep.*
70. Suresh G, Seenivasan G. 1997. *Nuclear Mater.* 249:259
71. Suresh G, Seenivasan G. 1998. *J. Alloys Compounds* 269:L9
72. Deleted in proof
73. Maloney MJ. 2001. *U.S. Patent No.* 6,177,200
74. Yokokawa H, Sakai N, Kawada T, Dokiya M. 1990. *J. Am. Ceram. Soc.* 73:649–58



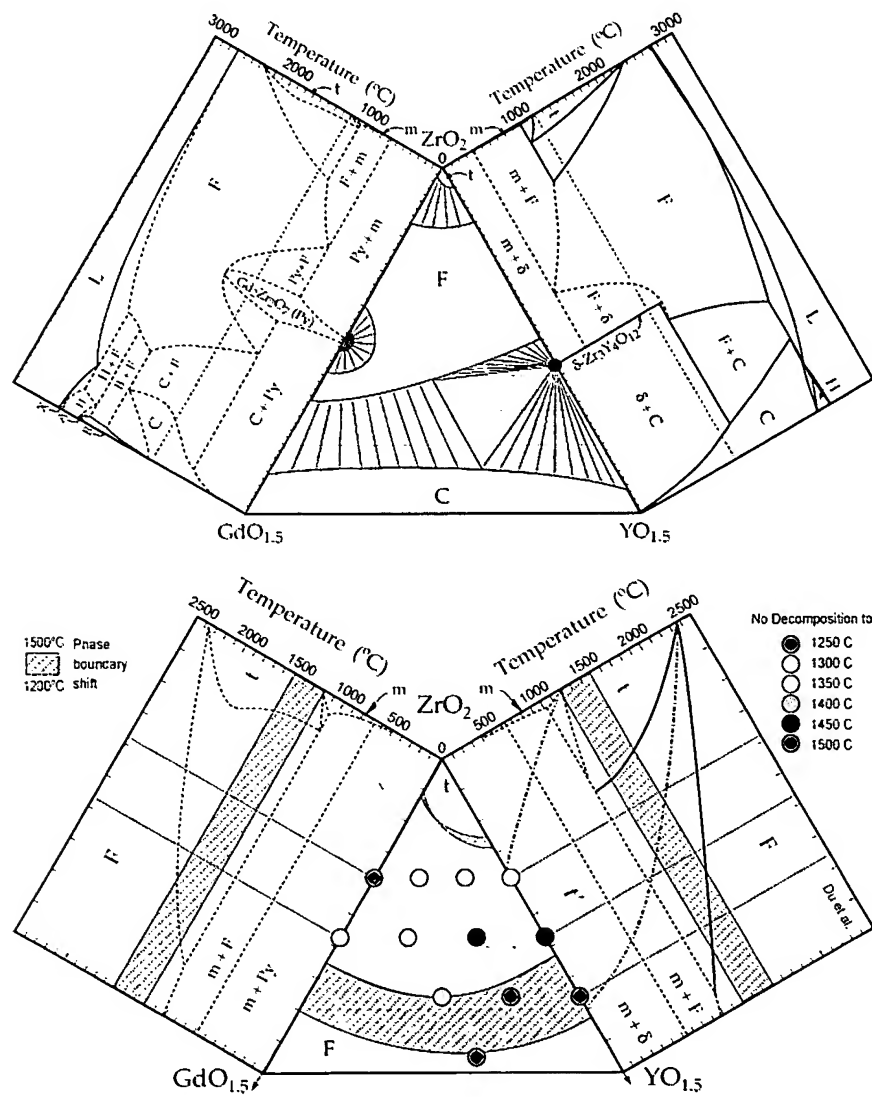


**Figure 17** (top) Representation of the  $\text{ZrO}_2$ - $\text{YO}_{1.5}$ - $\text{GdO}_{1.5}$  ternary diagram (37). (bottom) The zirconia-rich portion of the ternary diagram. The coloration of the dots represents the highest temperature at which no decomposition of the tetragonal-prime phase is observed (37).

a)

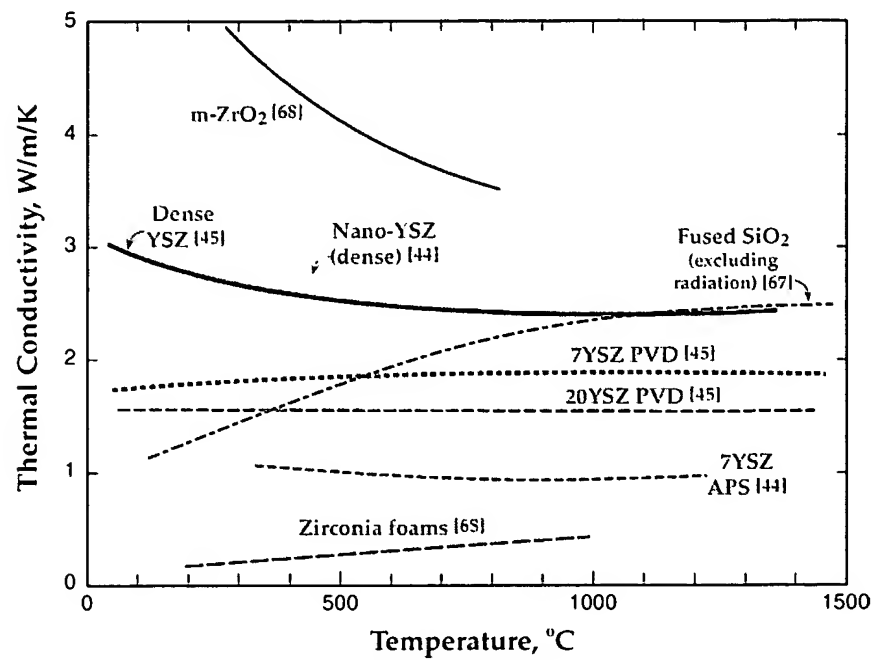


**Figure 20** (a) Thermal conductivity of a number of zirconia coatings, prepared by physical vapor deposition and air plasma spraying. The thermal conductivity of fused silica and zirconia foams are shown for comparison.

b)

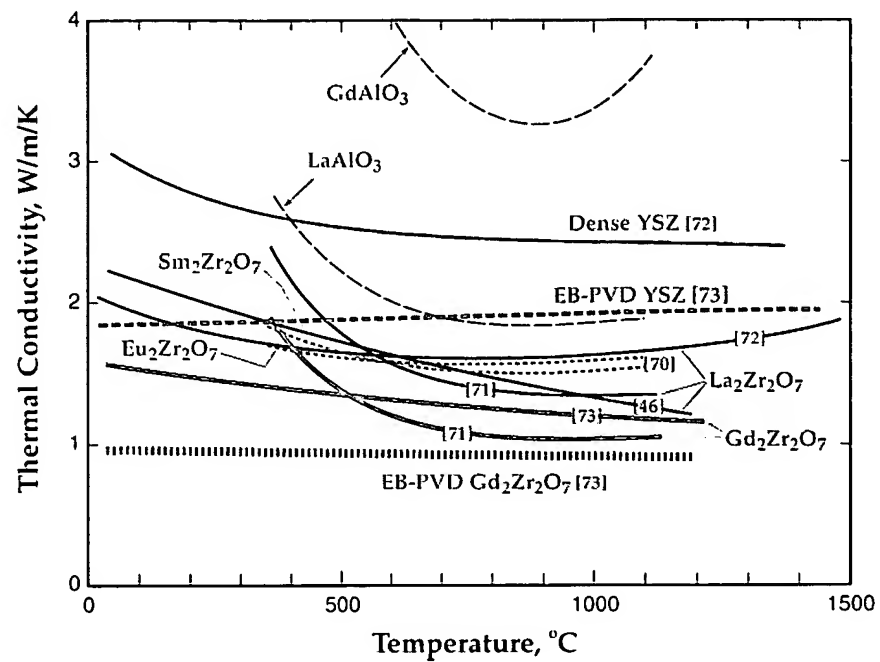


**Figure 20** (b) Comparison of the thermal conductivity of a number of aluminates, zirconates and zirconia coatings. (Numbers in brackets refer to references.)



# Emerging materials and processes for thermal barrier systems

Carlos G. Levi \*

*Materials Department, University of California, Santa Barbara, CA 93106-5050, USA*

Accepted 23 March 2004

## Abstract

Thermal barrier systems have been the subject of vigorous research and development activities over the past few years, driven by the demands for enhanced reliability and substantially higher operating temperatures envisaged for the next generations of gas turbine engines. The menu of candidate materials and architectures has expanded considerably, including numerous concepts based on zirconia as well as radically different materials, multilayers and modulated distributions of porosity and chemical composition. Advances in deposition processes enable increased flexibility for tailoring composition and microstructure to local requirements within the coating system, e.g. for thermal insulation, control of interdiffusion, enhanced resistance against environmental degradation and condition monitoring. Many challenges remain but healthy and growing collaborations between the science and technology communities bode well for future progress in this area.

© 2004 Published by Elsevier Ltd.

## 1. Introduction

The past decade has seen the emergence of engineered coating systems as arguably *the* crucial materials problem for the next generation of gas turbine engines [1]. First adopted simply as a means to enhance the durability of metallic components in the hostile engine environment, coatings are now envisaged as prime-reliant elements in design, essential to extend the performance limits of current alloys as well as to enable the utilization of ceramics in gas turbines. Specifically, thermal barrier coatings (TBCs) offer a quantum leap in temperature capability equivalent to three decades of progress in alloy design, processing and cooling engineering [2], but reliability concerns have largely limited their use to reducing the effective temperature of the metallic component and thus extending its life [3]. Current engine design goals, however, are unlikely to be met unless major advances are made in both coating reliability *and* performance. Moreover, candidates to replace superalloys in the longer term, e.g. refractory silicides and ceramics, are now acknowledged to require both thermal and environmental barriers for their implementation [4,5]. Recognition of the latter need is rather recent, motivated by engine tests [6,7] that

brought into light the full magnitude of the moisture attack problem on silicon-based ceramics [8]. The result of these trends has been a marked increase in TBC research activity, with approximately half of the total number of publications over the last 30 years <sup>1</sup> appearing after the last Current Opinion review on this subject [9].

A substantial number of reviews on various aspects of TBCs are found in the recent literature, e.g. [10–16]. In combination, they reflect a field evolving from a successful technology built largely on a heuristic foundation, with a small menu of materials and largely preoccupied with reliability, to an increased emphasis on the scientific understanding of the dynamics of these systems, the development of mechanism-based models and the diversification of materials to address the performance and durability demands of new generations of engines. In an effort to complement recent reviews and minimize overlap, this paper focuses on materials and process developments primarily aimed at enhancing performance, with selected comments on relevant durability issues. The emphasis is on the thermal barrier (Fig. 1) because it represents the area with greater diversity of alternate material concepts emerging in the period under review (not surprisingly since current

\* Tel.: +1-805-893-2381; fax: +1-805-893-8486.

E-mail address: [levic@engineering.ucsb.edu](mailto:levic@engineering.ucsb.edu) (C.G. Levi).

<sup>1</sup> Based on a SciFinder Scholar search for references under the topic “thermal barrier coatings”.

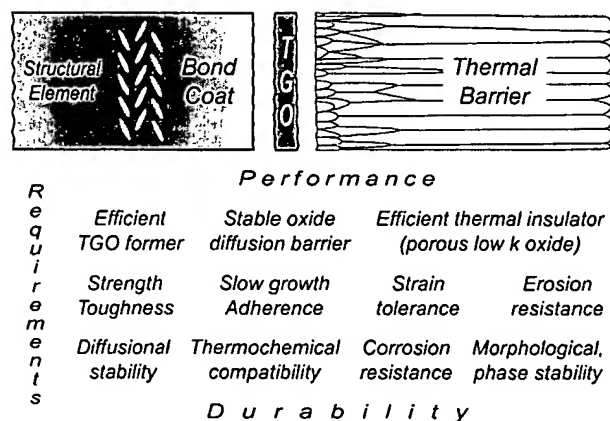


Fig. 1. Schematic of a thermal barrier system showing constituent elements and major requirements for performance and durability.

technology is based essentially on a single material). Selected developments in bond coats are briefly reviewed but justice cannot be done to the importance of the subject within the scope of this paper. The reader is referred to [14] for a recent and more extensive review on bond coats.

## 2. The thermal barrier system

The generic constituents of a thermal barrier system for a superalloy component are illustrated in Fig. 1, along with a summary of requisite attributes for performance and durability. The baseline thermal barrier or "top coat" is a 125–250  $\mu\text{m}$  layer of porous  $\text{ZrO}_2$  partially stabilized with  $7 \pm 1$  wt.%  $\text{Y}_2\text{O}_3$  (7YSZ), applied by either air-plasma spray (APS) or electron-beam physical vapor deposition (EB-PVD). Environmental protection relies primarily on a thin (<10  $\mu\text{m}$ ), dense  $\text{Al}_2\text{O}_3$  layer (TGO), grown during service by thermal oxidation of the underlying metal. (Concepts for additional environmental barriers exist, e.g. for protection against the attack of molten deposits, but none has become part of the baseline system so far.) Because superalloys are optimized for mechanical performance, their surfaces must be modified chemically to promote the formation of a stable, adherent TGO. These modified surfaces or "bond coats" (BCs) are classified into two major groups: (i) single phase  $\beta$ -(Ni,Pt)Al (B2), applied by electrodeposition of Pt and subsequent aluminizing by some form of chemical vapor deposition (CVD) with concurrent interdiffusion, and (ii) overlay two-phase ( $\gamma + \beta/\gamma$ )  $\text{MCrAlY}$ 's, applied by low pressure plasma spray (LPPS) or by EB-PVD [14].

The most important development at the system level has been the emergence of a "systems perspective" [11], wherein functionality may be viewed as depending primarily on the attributes of the individual layers, whereas

durability is usually dominated by their interplay. Consequently, modeling has taken an increasingly prominent role not only as a tool for elucidating the underlying mechanisms but, more importantly, as the only viable approach to integrate the contributions of the multiplicity of complex phenomena occurring within the system. TGO growth and the associated evolution of stresses, damage and eventually spallation of the top coat upon thermal cycling continue to be the primary focus of the durability models [17–21]. Increased sophistication in the models has captured some of the effects of the neighboring layers on the critical TGO dynamics, e.g. [20,22,23] but the experimental evidence indicates that much remains to be done in this area. A notable example of the interaction between modeling and experimental work during this period relates to the development of displacement instabilities in the TGO [24] whose origin has been a subject of considerable debate and remains unresolved. Proposed contributions arise from cyclic plasticity in the BC and TGO [25,26], phase transformations in the bond coat [27,28], and the in-plane growth strain in the TGO [24]. The mechanism responsible for the latter has also been a subject of considerable interest and discussion during the review period [29].

## 3. Advances in thermal barrier materials and processes

Current technology is based essentially on one thermal barrier material, 7YSZ. The selection of this composition and its continued preference is a prime example of the predominance of durability over performance. Higher Y contents offer improved insulating potential [30,31] but 7YSZ showed superior cyclic life in early tests [32] and continues to prevail over novel materials based on similar criteria and its established processability by both APS and EB-PVD. While it is generally acknowledged that 7YSZ is yet to be utilized to its full potential, the search for alternate materials has intensified in the recent past, predicated primarily on the prospect of substantially higher operating temperatures. At issue are the ageing effects on the phase stability of 7YSZ above  $\sim 1200^\circ\text{C}$  [33,34], as well as on the pore content and architecture needed to achieve strain tolerance [35,36] and desirable reductions in the thermal conductivity ( $\kappa$ ) [37,38]. There is also a growing concern about various forms of attack associated with contaminants in the gas stream, including erosion [39–41], foreign object damage [42], loss of compliance by penetration of molten deposits [43,44], and de-stabilization by hot corrosion [45–47].

Much of the research on thermal barrier materials has been driven by the desirability of further reducing  $\kappa$  and improving microstructure stability at high temperature. The approaches taken can be broadly classified as

modifications to the chemical composition, pore content and architecture, or other aspects of the topology of the coating (layering, grain size, etc.), often through processing changes. Salient developments are reviewed below.

### 3.1. Processing

A number of notable concepts have emerged on the deposition technology for thermal barriers. Key trends arise from the disparate attributes of EB-PVD and APS coatings, the former offering greater durability [13,48] and the latter better insulation efficiency [49]. Accordingly, efforts on EB-PVD have focused on reducing the thermal conductivity toward APS values ( $\geq 1$  W/mK) by modification of the pore content and architecture through changes in process parameters. These include increasing the pressure [50] and the distance from the source [51] during deposition, applying an intermittent plasma to produce a modulation in density [49], periodically introducing a contaminant in the deposition atmosphere to break down and "re-germinate" the columnar growth at a smaller scale [52], and manipulating the substrate to produce a zig-zag pattern wherein the intercolumnar gaps are oriented obliquely to block more effectively the heat transport across the coating [53]. The last two approaches reflect an important change in the understanding of the pore architecture, wherein the intercolumnar gaps are no longer viewed only as the source of strain tolerance [54], but also as potential contributors to the thermal insulation. The minimum conductivities reported in all these cases are still  $\geq 1$  W/mK.<sup>2</sup>

The most radical innovation in EB-PVD technology is arguably the incorporation of high velocity gas flow to focus the vapor plume, known as "directed vapor deposition" (DVD) [55]. The early motivation for this approach was to improve the deposition efficiency but the ability to manipulate the carrier gas, the introduction of multiple sources and plasmas, and the potential for reactive deposition open a richer menu of synthesis opportunities for both BCs and TBCs. Conductivities for 7YSZ comparable to those of APS TBCs were reported on zig-zag microstructures produced by DVD [56]. A microwave plasma-enhanced CVD route has also emerged as a viable route to produce YSZ coatings with segmented columnar microstructures at rates competitive with established EB-PVD technology ( $\sim 4$   $\mu\text{m}/\text{min}$ ) [57,58]. Results reported so far, while promising, do not seem to offer a significant improvement in performance or durability over EB-PVD [59], but potential benefits are claimed in flexibility for depositing certain compo-

sitions, coating multiple parts, and lower investment and operating costs [57].

Two developments in APS technology are particularly notable. The first one is the maturation of the dense, vertically cracked (DVC) TBCs [60], wherein the incorporation of cracking patterns mimicking the segmentation of the EB-PVD coatings is intended to improve their strain tolerance [61]. The denser microstructure involves a reduction of the inter-splat porosity and thus a penalty in thermal resistivity but appears to benefit the erosion resistance [62,63], which is generally lower in APS than in EB-PVD [48]. By manipulation of the deposition parameters the DVC coating density can be reduced near the surface to facilitate polishing, as needed to optimize aerodynamics in airfoils [64]. These attributes have made DVC TBCs the technology of choice for larger turbine components, especially combustors and nozzles in advanced power generation [65].

A more recent deposition technology involves plasma spray of solution precursors (SPPS) [66]. The process yields a nano-structured deposit through a sequence of rapid solvent evaporation, pyrolysis and crystallization that may occur both in flight and on the substrate [67]. Initial reports claim significant improvements in cyclic durability over other APS methods and even over EB-PVD [68], ascribed to a DVC-like microstructure. The thermal conductivity is significantly higher than that of conventional APS coatings ( $\sim 1.4$  W/mK) [66], but the approach offers the advantage of circumventing the need for powder feedstock and thus the ability to explore multiple compositions expeditiously and at relatively low cost.

Progress in the fundamental understanding of the TBC deposition processes has been substantial in the recent past. The mechanisms responsible for the different types of porosity in EB-PVD coatings have been elucidated [69–71], revealing the multiple scales at which the features of the growth front interact with the incident vapor. More significantly, it has been shown that shadowing plays a critical role (previously not appreciated) on the selection of in-plane and out-of-plane textures in columnar coatings [69], as well as on inducing microstructure variability. The latter results from variations in the local vapor incidence pattern produced by interactions of the flux with the geometry of the component [69,72]. Recent developments in characterization techniques [73] open new vistas for property prediction and process optimization by generating the requisite quantitative information about these complex microstructures.

### 3.2. Alternate low $\kappa$ materials

The major trends in novel compositions for reducing and/or stabilizing the thermal conductivity are based on  $\text{ZrO}_2$  modified by rare-earth (lanthanide) oxide (REO)

<sup>2</sup> Care should be exercised in comparing the claims regarding reductions in thermal conductivity since details about the condition of the sample (as-deposited vs. aged, aging treatment, etc.) are often missing.

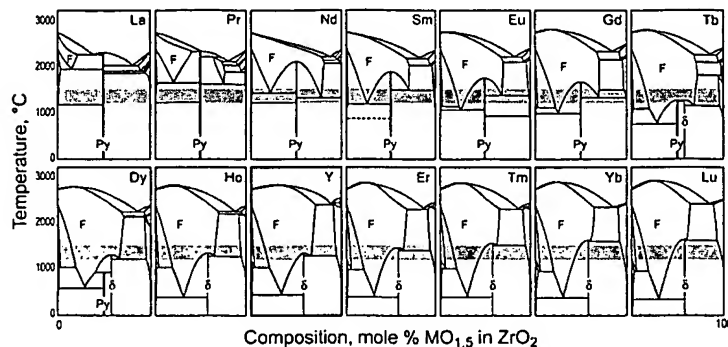


Fig. 2. Calculated phase diagrams for  $\text{ZrO}_2\text{-REO}_{1.5}$  binary systems, adapted from Yokokawa [166]. The  $\text{ZrO}_2\text{-YO}_{1.5}$  system has been inserted in the Lanthanide series for comparison. Note the systematic changes with decreasing size of the RE cation (from La to Lu), including the expansion of the fluorite field, the gradual de-stabilization of the pyrochlore phase ( $\text{M}_2\text{Zr}_2\text{O}_7$ ) and its replacement with the  $\delta$ -zirconate phase ( $\text{M}_4\text{Zr}_3\text{O}_{12}$ ).

additions, reflecting the still unsuccessful search for alternate base oxides with demonstrated overall superiority over zirconia. Preliminary calculations of the  $\text{ZrO}_2\text{-LnO}_{1.5}$  phase equilibria [74] reveal strong similarities with  $\text{ZrO}_2\text{-YO}_{1.5}$  (Fig. 2) and well-behaved trends with ionic size, especially on the extent of the fluorite field and the stability of the zirconates. Thermal conductivity calculations using a semi-empirical phonon model [75] further suggested a nearly linear trend of decreasing  $\kappa$  with increasing cation size between Sc and La, with an approximate slope of  $-2.9 \text{ W m}^{-1} \text{ K}^{-1} \text{ \AA}^{-1}$  for stabilizer contents of 0.08 and 0.18  $\text{MO}_{1.5}$  [13]. Lanthanide additions thus offer the dual opportunity to explore the design space in a systematic manner and to develop fundamental insight into the relative contributions of ion size and mass to the phonon transport processes.

Two important groups of candidate low  $\kappa$  materials have thus emerged, one based on co-doping of YSZ with one or more REO [76–79] and the other on the pyrochlore-type zirconates ( $\text{M}_2\text{Zr}_2\text{O}_7$ ) in Fig. 2 [80–84]. A comparison of selected results for EB-PVD coatings is given in Fig. 3, wherein the baseline (dashed curve) is given by the average trend for YSZ materials with increasing Y content [76]. (Variability can be significant, as noted by the control 7YSZ and 20YSZ samples for different studies.)

The more extensive results reported in the literature are on multiple co-doping of TBCs, typically comprising Y plus two other cations, one smaller (Yb, Sc) and one larger (Sm, Nd, Gd) [77,78]. These have been designated as “defect cluster systems” on the basis of TEM obser-

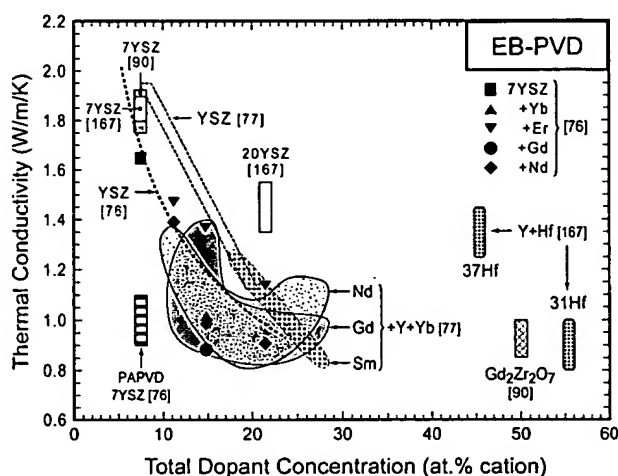


Fig. 3. Comparative summary of thermal conductivity values reported in the literature for a variety of zirconia-based materials, from [76,77,90,167].

vations showing nano-scale clustering of the smaller and larger cations in different regions, with Y being uniformly distributed [78]. It was proposed that these clusters contribute to phonon scattering and are primarily responsible for larger reductions in conductivity than those found with Y alone or co-doped with only one of the cations of interest (at comparable total dopant concentration). However, reductions in  $\kappa$  of similar magnitude were reported in a parallel study [76] on systems co-doped with  $7\text{YO}_{1.5}$  and an equivalent amount of only one REO<sub>1.5</sub>, especially Gd (cf. Fig. 3).<sup>4</sup> The latter were ascribed to a combination of phonon

<sup>3</sup> The relevant effects of alloying in  $\text{ZrO}_2$  are based on the extent of cation substitution and thus the convention of expressing concentrations as atomic percent cation (mole percent of half-formula-unit for sesquioxides) is adopted here. In the opinion of the author this should be the standard practice in the TBC literature to allow rigorous comparison of results and to provide a consistent framework for analysis.

<sup>4</sup> The conductivities in [77,78] were measured under large gradients wherein the outer surface temperature is above  $1200^\circ\text{C}$  [85], whereas those in [76] were measured with a standard laser flash technique at essentially uniform and much lower temperature ( $\leq 500^\circ\text{C}$ ). However, the temperature variation of conductivity is modest in all these materials and thus the comparison is, to a first approximation, still appropriate.

scattering point defects and “colouring” effects that reduce the radiative component of thermal transport within the TBC. In addition to the uncertainty in the mechanism(s) responsible for the reduction in conductivity, it is noted that there is no clear trend emerging from these studies regarding the postulated effects of ionic size or mass on  $\kappa$ . The inference is that the effect of doping on  $\kappa$  may be masked by the contribution from porosity [86], which could also vary with composition because of its influence on the kinetics of surface diffusion. Reported reductions in the rate of thermal resistivity degradation upon aging, associated with REO co-doping [77], are consistent with this view. Proper comparison of fully dense specimens is hindered by the sluggish sintering and the need to limit the densification temperature to prevent de-stabilization of the  $t'$  structure (see below).

Pyrochlore oxides ( $A_2B_2O_7$ ) are a relatively new addition to the menu of TBC materials: the first patent application was filed in 1996 [80]. Of particular interest are the zirconates of the larger lanthanides ( $Gd \rightarrow La$ ), which are phase-stable up to at least 1500 °C (Fig. 2). Several other attributes make these materials attractive. An increased level of substitution relative to the co-doped compositions (from <15% to 50% $MO_{1.5}$ ) and the use of cations with a much higher atomic mass contrast with Zr than Y [87], are expected to yield a substantial reduction in  $\kappa$  relative to 7YSZ [80]. Indeed, thermal conductivities ranging from  $\sim 1.1$  to  $\sim 1.7$  W/mK at temperatures between 700 and 1200 °C have been reported for zirconates of Gd, Eu, Sm, Nd and La [82,83,88–91]. Within this range, however, there are discrepancies among the different studies owing to the presence of significant residual porosity in the nominally “dense” specimens as well as the details of the measurement technique. When used as coatings these materials further benefit from the presence of porosity, as illustrated for  $Gd_2Zr_2O_7$  in Fig. 3 [90]. Because they also exhibit sluggish sintering kinetics [82,92], they tend to preserve their pore content and architecture to higher temperatures, with concomitant benefits to the long-term strain tolerance and insulating efficiency.

Some additional observations on the thermal conductivity of zirconates are of interest. Measurements on dense  $Gd_2Zr_2O_7$  compacts suitably heat treated to yield the pyrochlore and fluorite allotropes of the compound revealed no significant effect of ordering on the thermal conductivity [83]. Moreover,  $\kappa$  was found to vary only slightly over a wide range of  $ZrO_2$ – $GdO_{1.5}$  compositions away from the pyrochlore stoichiometry, especially at high temperature [93]. Although measurements were limited to  $\leq 700$  °C in these studies, molecular dynamics (MD) simulations predict the extension of this effect to higher temperatures (1400 K) for  $GdO_{1.5}$  and  $YO_{1.5}$  additions to  $ZrO_2$  [94]. The inference is that these materials behave essentially as heavily doped zirconias,

wherein  $\kappa$  is relatively insensitive to concentration above a certain value because of increasing interactions between the point defects. Co-doping of pyrochlores on both A and B sites has been proposed to further reduce their conductivity and modify their thermal expansion coefficient [91,95]. Notably, doping of  $La_2Zr_2O_7$  with 30% Nd, Eu or Gd revealed a systematic variation with ionic mass of the dopant cation and yielded a maximum reduction in  $\kappa$  from  $\sim 1.55$  to  $\sim 0.9$  W/mK for Gd at 800 °C. Conversely, fully dense stoichiometric Nd, Sm and Gd zirconates [83] and 97% dense  $La_2Zr_2O_7$  [82] were found to have essentially the same conductivity ( $\sim 1.5$ – $1.6$  W/mK) at 700 °C, supporting the existence of a true co-doping effect. The contribution of the porosity, however, remains to be fully quantified.

Numerous low  $\kappa$  compositions have been proposed beyond the  $ZrO_2$ – $REO_{1.5}$  systems. Notable non- $ZrO_2$  examples include  $CeO_2$ – $YO_{1.5}$  [96,97],  $La_2Ce_2O_7$  [98], La hexa-aluminate ( $LaMgAl_{11}O_{19}$ ) [99,100] and more broadly magnetoplumbites ( $LnM_{1+x}Q_xAl_{11-2x}O_{19}$  where  $Ln^{3+} = La \rightarrow Gd$ ,  $M^{2+} = Sr$ ,  $Mn \rightarrow Zn$ ,  $Q^{4+} = Ti$ ,  $Si$ ) [101], Garnets ( $Y_3Al_xFe_{5-x}O_{12}$ ) [102], and Monazite ( $LaPO_4$ ) [103]. The  $LaMgAl_{11}O_{19}$  materials are of particular interest for taking advantage of a plate-like structure that exhibits anisotropic diffusion (and by extension coarsening) and leads in practice to non-densifying microstructures [99]. Additional concepts discussed later involve tailored microstructures, e.g. by layering alternate compositions.

The search for improved TBC materials has highlighted the paucity of understanding and predictive models for thermal transport at high temperature, especially in chemically and microstructurally complex materials such as TBCs. Accordingly, substantial effort has been placed on adapting and further developing earlier phonon models to this application, e.g. [13,16,75, 93,104]. Improved understanding of the contribution of point defects has emerged from these efforts and the models can explain some experimental results, but quantitative agreement is often elusive. MD simulations [94,105] show promise, as noted above, but full validation of the models is still in progress. For example, calculations for La-, Nd-, Sm- and Gd zirconates at  $\sim 1200$  °C predict  $\kappa \sim 1.9 \pm 0.1$  W/mK [94,105], essentially independent of the A cation. By comparison, experimental measurements at  $\sim 700$  °C give  $\kappa \sim 1.6$  W/mK for the same materials, but a somewhat wider spread at 1473 K ( $\sim 1.2$  W/mK for  $Gd_2Zr_2O_7$  [90] to  $\sim 1.7$  for  $La_2Zr_2O_7$  [82]).

A “user friendly” model aimed at providing first order guidelines for the development and selection of alternate TBC materials was proposed recently [86]. The premise is that the relevant temperatures are well above the Debye temperature for most materials of interest and thus the intrinsic thermal conductivity should be approaching a minimum value, largely independent of



point defects [106,107]. Candidate TBCs should then be compared on the basis of their “minimum thermal conductivity”, as that represents the lowest value achievable for a given material [86]. (Radiative contributions that would enhance the conductivity of translucent materials at high temperature are neglected in this approach, as are the contributions of optical phonons.) The expression for the  $\kappa_{\min}$  given in this work can be conveniently rewritten as:

$$\kappa_{\min} \rightarrow 0.87 k_B \bar{\Omega}_a^{-2/3} (E/\rho)^{1/2} \quad (1)$$

where  $\bar{\Omega}_a = [M/(m\rho\mathcal{N}_A)]$  is the average volume per atom,  $E$  is the elastic modulus,  $\rho$  is the density,  $M$  the molar mass,  $m$  the number of atoms per formula unit,  $\mathcal{N}_A$  is Avogadro's number and  $(E/\rho)$  is proportional to the acoustic velocity. A logarithmic plot of  $\kappa_{\min}$  against  $(E/\rho)$  at constant  $\bar{\Omega}_a$  should be linear, suggesting the development of an Ashby-type map for comparing candidate TBC materials—see Fig. 4(a). It is evident that the materials of greater interest cluster on the lower left corner of the graph and have clear advantages over alternate oxides such as Zircon, Spinel, Mullite and YAG that have also been proposed in the literature. Since theoretical density and average atomic volume can be calculated with substantial precision for known materials, the main uncertainty in this plot is on the elastic modulus. The potential error, however, is ameliorated by the half power dependence of  $\kappa$  on  $E$ .

A comparison of calculated and measured  $\kappa_{\min}$  values is given in Fig. 4(b). As expected, all experimental values are above their calculated  $\kappa_{\min}$ , with the deviation a measure of the maximum potential for improvement. Note that the RE zirconates appear unexpectedly close to the limit, arguably because the minimum values in the literature are for materials that, while labeled nominally dense, still contain some porosity. It is, of course, possible that some materials have not yet reached the regime of the minimum conductivity (obscured perhaps by the onset of radiative transport) and thus point defects may be playing a role. The qualitative guidelines emerging from this work are that candidate low  $\kappa$  materials should contain larger, heavier ions, compliant bonds and structural disorder [86].

### 3.3. Issues with low $\kappa$ TBCs

Thermochemical compatibility with the underlying alumina should be a primary requirement for any top coat material, since any reaction that consumes the TGO would likely replace it with a less protective oxide. The prototypical scenarios are depicted in Fig. 5. The tetragonal form of  $\text{ZrO}_2$  exhibits two-phase equilibria and only minimal solubility with  $\alpha\text{-Al}_2\text{O}_3$  at the expected upper temperature limit for the TGO/TBC

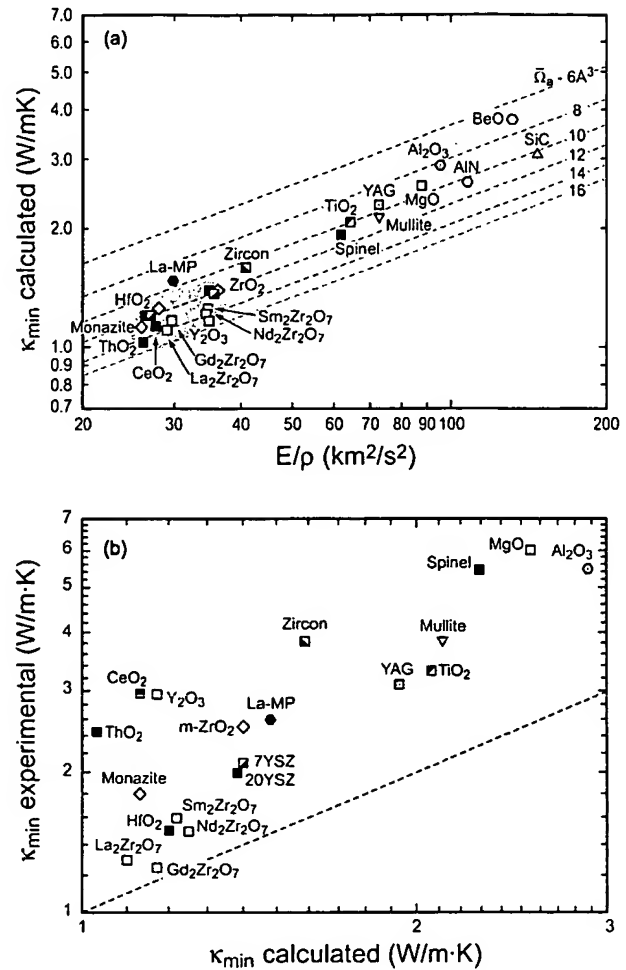


Fig. 4. Minimum thermal conductivity values for materials of interest in thermal barrier coatings, including other common ceramics for comparison: (a) calculated  $\kappa_{\min}$  from Eq. (1), based on [86] and (b) comparison with experimental values, taken as the lowest value reported in the literature for a nominally dense material.

interface ( $\sim 1200$  °C).<sup>5</sup> This compatibility extends partially to the cubic field for Y and all but the larger Lanthanides, for which no cubic field is present on the binary at the temperatures under discussion (cf. Fig. 2). The equilibrium breaks down at some critical concentration ( $X^*$  in Fig. 5) beyond which the diffusion path would lead to the formation of one or more interphases.

Three types of situations arise. For Y and the smaller lanthanide cations the first aluminate to form upon saturation is a Garnet (Fig. 5a) whereas the larger lan-

<sup>5</sup> Substantial mutual solubility, however, is known to occur with metastable aluminas [108] such as those that form in the early stages of oxidation for some bond coats, e.g. [109,110]. It has been proposed [111] that this could lead to the formation of the “mixed alumina/zirconia zone” sometimes observed at the TGO/TBC boundary [10], with possible implications for the durability of the system. The mechanisms and effects remain under investigation.

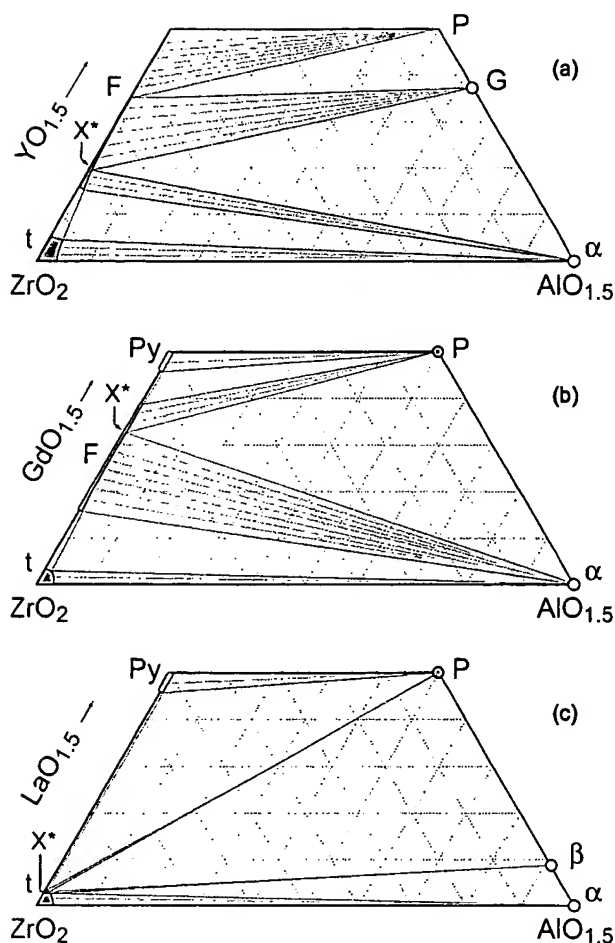


Fig. 5. Preliminary phase diagrams depicting the various scenarios for interaction between the TGO and  $\text{ZrO}_2\text{-REO}_{1.5}$  materials, where  $X^*$  is the maximum tolerable concentration to avoid interphase formation at  $\sim 1200^\circ\text{C}$ . The expected interphases as  $X^*$  is exceeded are: (a) Garnet (G); (b) Perovskite (P) and (c)  $\beta$  alumina. Sources cited in text. F = cubic  $\text{ZrO}_2$  (fluorite), t = tetragonal  $\text{ZrO}_2$ , Py = pyrochlore.

thanides (La, Nd, etc.) form instead  $\beta$ -alumina at much lower concentrations of  $\text{REO}_{1.5}$  (Fig. 5c). Gd and possibly its immediate neighbors do not form either of the higher aluminates, whereupon the perovskite phase would be the expected first product of interdiffusion above  $X^*$  (Fig. 5b). While most of these ternary systems are still under investigation, current understanding suggests that the differences above translate into different degrees of tolerance of the TGO to dopant content in the TBC, with  $X^*$  being lowest for La (probably  $< 5\%$  at  $1200^\circ\text{C}$ ), highest for Gd ( $\sim 34\%$  at  $1200^\circ\text{C}$  [112]) and intermediate for Y ( $\sim 20\%$  at  $1250^\circ\text{C}$  [113]). The implication is that all the pyrochlore zirconates are prone to degrade the TGO by interdiffusion, requiring incorporation of a compatible “diffusion barrier”, typically 7YSZ, for safe implementation. Such underlayers are mentioned in the zirconate patent literature dating back to the first filing [80,92,114], but usually justified in

terms of adhesion, toughness or thermal expansion mismatch, with no discussion of the thermochemical compatibility problem. The dual-layer structures present some challenges for implementation in the current industrial-scale EB-PVD systems, which are typically designed with multiple sources but operating with only one source material. The nearly invariant thermal conductivity over a wide range of intermediate compositions in  $\text{ZrO}_2\text{-GdO}_{1.5}$  [93] opens the possibility of lowering the Gd content of the TBC below  $X^*$  (Fig. 5b), rendering the interface compatible without a significant penalty in thermal conductivity relative to the pyrochlore. Conversely, a proposed composition for improved sintering resistance based on a minimum content of  $31\%\text{YO}_{1.5}$  [115] would clearly be susceptible to thermochemical interaction with the TGO (Fig. 5a).

In contrast with the RE zirconates, the leaner Y + RE co-doped compositions should be generally compatible with the TGO (with precise limits to be determined), but are not fully phase stable at the temperatures of interest. Figs. 6 and 7 illustrate the origins of the problem. Results of cyclic tests available in the literature reveal that, with few exceptions, optimal durability within a given chemistry occurs at low dopant concentrations (Fig. 6). This led to the early selection of 7YSZ as the preferred TBC composition for APS coatings notwithstanding its non-optimal  $\kappa$ , as noted before [32]. Remarkably, the trend is found to extend to other materials and processes including EB-PVD YSZ [116], APS YbSZ [117], 7YSZ co-doped with Hf [118] and most recently the “cluster” co-doped systems [119] (Fig. 6). With the exception of the APS Yb–Y–RE compositions in Fig. 6, wherein the highest values remain to be confirmed by further tests, the maxima for the different groups are all likely to fall

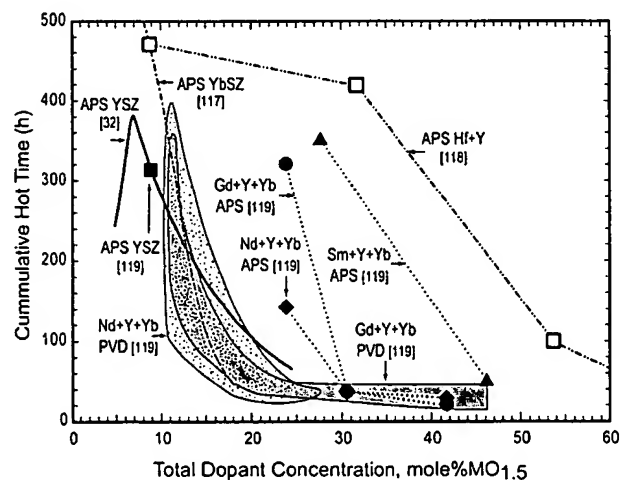


Fig. 6. Comparison of cyclic life for TBC materials where information is available in the literature. From [32,117–119]. Reported cyclic life has been converted to cumulative hot time to allow comparison between tests that used different hold times.

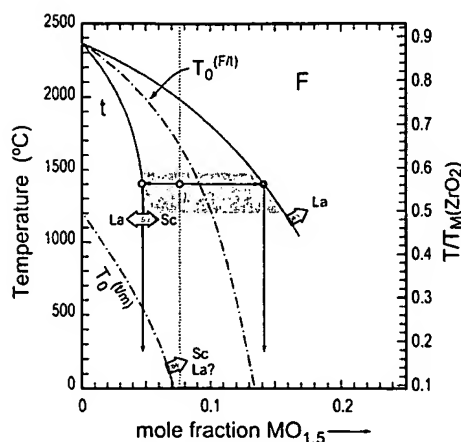


Fig. 7. Schematic ZrO<sub>2</sub>-MO<sub>1.5</sub> diagram illustrating the problem of t' phase de-stabilization upon thermal exposure and the relevant trends in the phase boundaries as well as the T<sub>0</sub> temperature for the tetragonal-monoclinic partitionless transformation, which represents an upper bound to the martensite start temperature.

within the t + F<sup>6</sup> or t + Py fields of the corresponding equilibrium diagrams (cf. Fig. 2). However, the coatings are typically single phase (designated t' or c' to denote supersaturation) in the as-deposited condition and thus susceptible to decomposition into the equilibrium assemblage upon exposure to the temperatures of interest.

Two important implications arise from the metastable nature of 7YSZ and related co-doped materials. A minimum dopant content, dictated conceptually by the intersection of the T<sub>0</sub>(t/m) curve with ambient temperature (Fig. 7), is needed to render the coating “non-transformable”, i.e. insensitive to the disruptive t ↔ m transformation upon thermal cycling. To a varying degree, the position of the T<sub>0</sub>(t/m) curve is uncertain for the systems of interest although the limited literature [120,121] suggests that Y represents a lower limit and the T<sub>0</sub>(t/m) curve shifts to higher compositions for both smaller (e.g. Sc) and larger (e.g. La) cations. Because the minimum dopant content for stability is in all relevant cases above its equilibrium solubility in the tetragonal phase, a second implication is that the equilibrium tetragonal phase resulting from partitioning of the as-deposited t'/c' structure would be “transformable” and thus jeopardize the long term durability of the coating [33].

The relative effect of different trivalent stabilizers on the resistance of TBC materials against partitioning and the ensuing monoclinic transformation is summarized in

<sup>6</sup> The cubic zirconia solid solution is labeled F (fluorite) to distinguish it from the cubic rare-earth oxide structure, which is normally designated as C. However, the term c' will be used to denote the supersaturated cubic zirconia form for consistency with the literature.

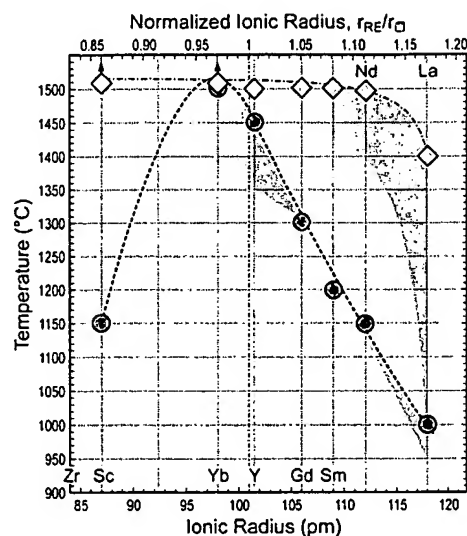


Fig. 8. Phase stability of singly doped binary ZrO<sub>2</sub>-MO<sub>1.5</sub> compositions (circles) and co-doped ZrO<sub>2</sub>-(Y<sub>0.5</sub>Mo<sub>0.5</sub>)O<sub>1.5</sub> compositions (diamonds). The curves represent the maximum temperature before significant monoclinic formation was observed, and the shaded areas the temperatures where some partitioning was observed without significant monoclinic evolution upon cooling. Co-doped compositions showing no sign of instability at 1500 °C (empty diamonds) are not expected to decompose at higher temperatures as they would enter the single phase cubic field. (Adapted from [168].)

Fig. 8. The phase stability of singly doped zirconias at constant dopant concentration (7.6%) shows a strong dependence on cation size, being optimal for Yb, Y (which interestingly match nearly the size of the coordinating oxygen cube), and declining for both larger and smaller cations. The trend for the larger cations was rationalized in terms of an increasing driving force for partitioning, reflected in the progressive displacement of the tetragonal boundary to lower concentrations with increasing cation size [122,123] (Fig. 7) and a concomitant widening of the t + F phase field. Conversely, the shift of the tetragonal boundary to higher concentrations for smaller cations [121] renders 7.6%ScSZ essentially insensitive to partitioning at ~1400 °C but the concurrent shift in the T<sub>0</sub>(t/m) curve makes this composition “transformable” upon cooling. This is at variance with the established view that Sc is a more effective stabilizer than Y [34,124], derived from experiments at higher concentrations and involving combinations of Y and Sc. Note, for example, that co-doped 7.6Y + 7.6Sc in Fig. 8 exhibits much higher stability than the singly doped material, but essentially the same as that for 15.2Y as both compositions are close to the cubic phase field boundary. The stability of co-doped compositions diminishes for the larger cations at similar stabilizer contents (Fig. 8), and can be further reduced when the RE cation predominates [125]. Co-doping can thus be designed to alleviate phase stability concerns, but not yet the problem of reduced cyclic durability (Fig. 6)

whose origins remain elusive. This represents one of the salient intellectual challenges for the TBC community today.

Additional issues arise when considering environmental effects on novel TBC materials. Various reports at conferences have suggested that alternate compositions generally exhibit lower erosion resistance than 7YSZ. For example, the following relative rates for particle erosion were measured in EB-PVD coatings: 20YSZ (129),  $\text{CeO}_2$  (35),  $12\text{YCeO}_2$  (22), 12YSZ (2.3), 7YSZ (1) [96]. A cursory review of the patent literature also suggests a concern with the baseline erosion resistance of 7YSZ as gas turbine environments become more aggressive [126]. The concerns have motivated recent modeling and experimental efforts to elucidate the mechanisms of erosion [39–42] and the role of the TBC properties on resistance to erosion and foreign object damage (FOD) [127]. Preliminary results suggest that the materials exhibit plastic deformation at service temperatures and also that there are significant differences in their yield properties, which could bear on their erosion resistance [127]. Approaches have also been proposed to increase the erosion resistance of TBCs by dispersion of a second phase oxide, e.g.  $\text{Al}_2\text{O}_3$  or  $\text{Cr}_2\text{O}_3$  [128,129]. These concepts address the limitations of earlier proposals involving discrete “wear” over-layers of, for example,  $\text{Al}_2\text{O}_3$ , [130] which would be more susceptible to spallation because of the thermal expansion mismatch with the TBC. While improvements have been reported, TBC erosion remains an area of strong interest and growing research.

Concerns related to the attack of molten silicate [44] or sulfate/vanadate deposits [47] on current TBCs are not particularly alleviated by alternate compositions. Molten calcium–magnesium–alumino-silicate deposits (CMAS) appear to readily penetrate all zirconia-based compositions (Kraemer et al. unpublished research) and probably most other TBC candidate materials. Conversely, the free energies of formation of rare earth vanadates are found to increase (become more negative) systematically with increasing radius of the RE cation [15], suggesting that many of the dopants of interest for reducing thermal conductivity would render the TBC even more susceptible to de-stabilization than 7YSZ. The corollary is that smaller cations like Yb and Sc should be more resistant to leaching by vanadate melts, in agreement with an earlier proposal of Sc as a preferred stabilizer when hot corrosion is a concern [124].

### 3.4. Multilayer concepts

A multilayer architecture is already the preferred approach to achieve multifunctionality in thermal barrier systems and is likely to persist and evolve further, e.g. [15], as demands for improved performance increase. Functionally grading the transition between the

bond and top coats, while conceptually appealing to diffuse the associated strain incompatibility, is now acknowledged to be ineffective because of the oxidation penalty resulting from intermixing the metal with the oxygen-transparent YSZ [131]. Grading the internal structure of the thermal barrier (and the bond coat), however, offers some interesting possibilities as detailed below.

Proposed multilayer approaches to the top coat may be broadly divided into three groups. The first one comprises discrete over-, under- or intercalated layers aimed at reducing the effect of interactions with the environment or with other elements of the system, notably the TGO.<sup>7</sup> Over-layers, often based on  $\text{Al}_2\text{O}_3$ , have been primarily intended for erosion [130] or corrosion protection [135,136]. Under-layers, typically 7YSZ, are aimed at enhancing the durability of alternate coatings [80,92,114]. Major issues have not been reported with 7YSZ under-layers since they are selected for their compatibility with the TGO and other  $\text{ZrO}_2$  based materials, and are deposited with strain-tolerant microstructures. However, dense over-layers are prone to delamination because of CTE mismatch and the lack of strain accommodation mechanisms. It is in this context that functionally graded architectures have been proposed, e.g. for increasing the resistance to CMAS attack [43]. This represents a departure from conventional thinking in that it accepts the attack of the outer TBC layer in order to achieve strain tolerance and thus its survivability until needed. The outer layer is endowed with a dispersion of particles, e.g.  $\text{Al}_2\text{O}_3$ , designed to dissolve into the molten CMAS and raise its melting point/viscosity hindering its penetration into the true “functional” TBC underneath. Conversely, erosion resistance is desirable throughout the coating and hence microstructural grading is not particularly advantageous. Design approaches in this case have evolved from intercalating a multiplicity of thin layers of the hard phase within the TBC [137] to alternating bands of dispersion hardened and normal 7YSZ [129] to a uniform dispersions of hard particles [128].

The second category of multilayer top coats is aimed at enhancing thermal insulation efficiency. One subset within this group was originally predicated on the potential scattering effect of interfaces, typically implemented by alternating thin layers of two distinct oxides

<sup>7</sup> Filling the intercolumnar gaps or coating their surfaces with a sintering inhibitor in EB-PVD TBCs [132–134] could arguably be considered part of this group, but the issues are somewhat different. Also included in this group are layers proposed to reduce oxygen ingress to the BC/TBC interface and thus the rate of TGO growth. These concepts are fundamentally hindered by the difficulties in reconciling the strain tolerance requirement with the need for a dense, continuous diffusion barrier that has a substantially lower  $\text{O}_2$  diffusivity than the TGO (otherwise one simply replaces part of a strain incompatible layer with another).

such as  $\text{Al}_2\text{O}_3$  and YSZ [138]. The concept presents a number of fundamental challenges, the most critical shared with an earlier proposal for using nanocrystallinity as a means to substantially reduce the thermal conductivity of YSZ. Notably, no significant contribution to  $\kappa$  from the interfaces was found in a study in which the layer thickness were systematically varied, down to 100–200 nm, consistent with the fact that the phonon mean free path in YSZ is already much smaller than practically achievable interface spacings [139]. Moreover, a separate study revealed that these layered structures are not as morphologically stable as originally expected, partly because of the occurrence of  $\text{Al}_2\text{O}_3$  in a transient form [140].

Related concepts based on layering of internal porosity within the columns have fared better although the underlying mechanisms are still under debate. One approach involves the periodic application of plasma discharge during EB-PVD [49], as noted before (cf. Fig. 3). The availability of multiple sources opens additional possibilities, for example by the creative use of two source materials with significantly different vapor pressures like 7YSZ and  $12\text{YCeO}_2$  [141]. The stability of the pore structure and ensuing increase in  $\kappa$ , however, remains an issue. An intriguing approach involves filling the pores in the outer layer of the coating with a gas or (partially) with a solid that prevents their densification [142]. The most recent version of this concept comprises alternating thin layers of  $\text{Ta}_2\text{O}_5$  or  $\text{Al}_2\text{O}_3$  within 20YSZ, with a suitable 7YSZ underlayer [143]. The concept accepts the breakdown of the layers into fine particles that, upon thermal cycling, are expected to debond from the matrix effectively appearing as “pores” to the heat flux. The deposition strategy concentrates pores in bands, which are calculated to be more effective in reducing  $k$  than a uniform distribution with the same volume fraction [143].

Layered architectures are also the foundation for managing the radiative heat transport in the coating system, especially important in combustor TBCs. Ideally the coating should reflect the majority of the incident radiation from the combustor, while allowing for transmission of any outward radiation originating at the substrate/coating interface [144]. A suggested approach is a dielectric stack comprising two ceramics of different refractive indexes with layer thickness depending on the desired wavelengths to be reflected and transmitted [144]. A further evolution of this concept incorporates a diffuse reflective layer comprising a bimodal distribution of ceramic particles (typically  $\text{Al}_2\text{O}_3$ ), pores and a silica binder, under the multilayer reflector [145]. Thin (1–3  $\mu\text{m}$ ) Pt-group metallic layers, preferably embedded within the TBC, have also been proposed for reflecting radiation [146]. As in other thin layers, morphological stability is likely to remain an issue, as well as oxidation in the case of metals.

A third group of multilayer concepts is motivated by the desirability of in-situ, non-contact monitoring of temperature and heat flux, as well as damage and/or residual thickness. A proposed avenue is to use the temperature-dependent luminescence properties of rare earths in a variety of relevant oxide hosts, notably Eu in YSZ or  $\text{Y}_2\text{O}_3$  and Dy in YSZ or YAG, to probe the coating temperature by measuring the life-time decay of the signal excited by a laser pulse [147]. These thermographic phosphors can be either applied as an external layer [148] or incorporated as a dopant into the TBC [147], the latter approach having the advantage of obviating thermomechanical or thermochemical incompatibilities and further contributing to reduce  $\kappa$ . A set up for mapping temperature distributions on the surface of an experimental combustor has been demonstrated [148]. In principle, the idea can also be used for measuring delamination-type damage that would result in local “hot” spots. Using layered architectures and multiple dopants enables the extension of the approach to monitor temperature at different places within the coating as well as the residual thickness [15]. Multilayer arrays of this type are under investigation (Clarke and Gentleman, unpublished research).

#### 4. Some remarks on bond coats

Improving bond coats continues to be regarded as the highest priority in current and emerging thermal barrier systems, as the potential of a higher performance thermal barrier can only be exploited if it remains adhered to the substrate. Moreover, some spallation is probably unavoidable in real operation even if the coatings were prime reliant because of events such as foreign object impact (R. Darolia, personal communication). A top coat with a substantially higher temperature capability would then require a similarly enhanced bond coat to ensure survivability of the component if local spallation occurs. However, the potential for increasing the BC capability is ultimately limited by the underlying superalloy, partly because temperature drops across the BC are much smaller than across the thermal barrier, and also because of exacerbated interdiffusion.

Major challenges in enhancing bond coat temperature capability are (i) to reduce the rate of TGO growth and the concomitant buildup of strain energy [11]; (ii) to increase the yield/creep strength and suppress cyclic plasticity effects [17]; and (iii) to minimize interdiffusion with the substrate that leads to Al depletion, upward migration of deleterious elements, and reduction in the effective thickness of the superalloy [14]. The relative importance of these challenges varies between the two main families of bond coats.

Salient developments in understanding TGO growth include a full appreciation of the importance of surface

condition prior to TBC deposition. The standard practice of grit blasting was found to introduce contaminants that accelerate TGO growth [149,150], and defects that can initiate interfacial separation [151]. A thin overlayer of Pt on grit-blasted NiCoCrAlY substantially enhanced TBC life in laboratory tests by shifting the BC/TGO interface away from the grit-blasted surface [151]. Persistent transient aluminas, generally undesirable in TBCs [111,152], were shown to transform more readily to  $\alpha$  by moderately increasing surface roughness [110]. Because of inherent limitations to the latter approach, alternate avenues suggested to accelerate the establishment of  $\alpha$ -Al<sub>2</sub>O<sub>3</sub> include elimination of other transient oxides [153] as well as inoculation or doping of the BC surface with elements that form oxides of similar crystal structure (Fe<sub>2</sub>O<sub>3</sub>, Cr<sub>2</sub>O<sub>3</sub>), combined with controlled pre-oxidation prior to TBC deposition [153,154]. The latter departs from the earlier notion that an initial oxide "consumed" part of the useful life of the system, generally thought of as linked to a critical oxide thickness [150]. Controlled pre-oxidation, however, can establish an oxide that subsequently thickens at a slower rate, with attendant benefits to the durability [154].

The search for stronger BCs has been substantially enhanced by the emergence of test methods that allow probing the real BC material, rather than monolithic alloys with similar composition [155]. The technique also allows in situ observation of the bond coat microstructure and phase transformations that influence its mechanical behavior [28]. Strengthening is a greater need in the  $\beta$ -NiAl base alloys but the options are also least compatible with current diffusion aluminizing techniques. Accordingly, a trend toward "overlay"  $\beta$  bond coats has emerged as a means to increase flexibility in alloy design and functional grading [156–160]. The approach is particularly attractive because it allows tailoring of the aluminide BC chemistry without relying on the superalloy to supply Ni or Cr. It is also possible to incorporate desired levels of solute/precipitation strengthening additions (Cr, Zr, Hf) [158], as well as "reactive" elements (Y, Hf, Zr) [156,160]. Of particular significance is the absence of Pt from some  $\beta$  alloy concepts [157], at variance with current art.

Effective BC/superalloy diffusion barriers have been an elusive goal [14]. The concept is, in principle, orthogonal to the established synthesis method for diffusion aluminides but the advent of an overlay approach for  $\beta$  alloys opens new opportunities in this area. Bilayer BC designs have thus emerged, with the outer layer tailored for optimum oxidation performance and the inner one to block interdiffusion. Ru alloys and intermetallics were identified as promising candidates in an extensive study of different materials based on diffusion couples [161]. In addition,  $\beta$ -RuAl offers advantages in refractoriness and mechanical properties over  $\beta$ -NiAl [162] and Ru additions could potentially be used for

strengthening aluminide bond coats. Some Ru-rich alloys are claimed to be sufficiently oxidation resistance to be suitable for protective coatings [163]. However, recent experiments on RuAl suggest reasons for concern (Rühle et al., unpublished work) although improved behavior is reported upon alloying [162]. Nevertheless, the patent literature emphasizes Ru-bearing alloys as diffusion barriers, with more standard Pt-modified aluminide at the TGO forming surface [164,165].

## 5. Outlook

The recent TBC literature reveals vigorous research and development activities combined with growing needs that bode well for the future of this field. It is not clear at this point what system architecture could replace the established combination of materials, but the numerous ideas put forward suggest an increased ability for designing the microstructure according to the local demands for functionality. Many concepts suggest the likely use of multilayers within both top and bond coats, either for control of interdiffusion, optimization of TGO formation, environmental protection or condition monitoring. Reflecting significant evolution in understanding, it is now recognized that desirable architectures are those that involve structural continuity, e.g. based on fluorite derived phases (with dopants or particle dispersions where needed) for the top coat, or single-phase  $\beta$  aluminides with locally tailored composition for the bond coat. Implementation of these ideas may require significant improvements in processing, but fundamental obstacles are not evident at this point.

It is also evident that the field has benefited from an increased collaboration between industry, government laboratories and academia, reflected in active interdisciplinary programs and a growing number of publications. Continued flourishing of these interactions has acquired even greater importance as the prospective complexity of future systems comes to light.

## Acknowledgements

The author is indebted to numerous colleagues in academia, industry and government laboratories whose input has contributed to his education on the subject of this review. The author is also grateful for research support that has enabled these interactions, including an international program for research collaborations sponsored by the National Science Foundation (DMR-0099695) and the European Commission (GRD2-200-30211), programs from the Office of Naval Research (N00014-99-1-0471 and MURI/N00014-00-1-0438), and the Alexander von Humboldt Foundation.



## References

- [1] NRC: Coatings for high-temperature structural materials: trends and opportunities. Washington, DC: National Academy of Sciences; 1996 [ISBN 0-309-05381-1].
- [2] Jones RL. Thermal barrier coatings. In: Stern KH, editor. Metallurgical and ceramic protective coatings. London: Chapman and Hall; 1996. p. 194–235.
- [3] Meier SM, Gupta DK. The evolution of thermal barrier coatings in gas turbine engine applications. *Trans ASME* 1994;116:250–7.
- [4] Bewlay BP, Jackson MR, Zhao J-C, Subramanian PR, Mendiratta MG, Lewandowski JJ. Ultrahigh temperature Nb-silicide-based composites. *MRS Bull* 2003;28:646–53.
- [5] Morrison JA, Merrill GB, Ludeman EM, Lane JE. Use of high temperature insulation for ceramic composites in gas turbines. US Patent, 6,197,424; 2001.
- [6] Kimmel J, Miriyala N, Price J, More KL, Tortorelli P, Eaton H, et al. Evaluation of CFCC liners with EBC after field testing in a gas turbine. *J Eur Ceram Soc* 2002;22:2769–75.
- [7] Lin HT, Ferber MK. Mechanical reliability evaluation of silicon nitride ceramic components after exposure in industrial gas turbines. *J Eur Ceram Soc* 2002;22:2789–97.
- [8] Opila EJ. Oxidation and volatilization of silica formers in water vapor. *J Am Ceram Soc* 2003;86:1238–48.
- [9] Wright PK, Evans AG. Mechanisms governing the performance of thermal barrier coatings. *Curr Opin Solid State Mater Sci* 1999; 4:255–65.
- [10] Stiger MJ, Yanar NM, Topping MG, Pettit FS, Meier GH. Thermal barrier coatings for the 21st century. *Zeit Metal* 1999;90: 1069–78.
- [11] Evans AG, Mumm DR, Hutchinson JW, Meier GH, Pettit FS. Mechanisms controlling the durability of thermal barrier coatings. *Progr Mater Sci* 2001;46:505–53.
- [12] Padture NP, Gell M, Jordan EH. Thermal barrier coatings for gas turbine engine applications. *Science* 2002;296:280–4.
- [13] Schulz U, Leyens C, Fritscher K, Peters M, Saruhan-Brings B, Lavigne O, et al. Some recent trends in research and technology of advanced thermal barrier coatings. *Aerospace Sci Technol* 2003; 7:73–80.
- [14] Nicholls JR. Advances in coating design for high performance gas turbines. *MRS Bull* 2003;28:659–70.
- [15] Clarke DR, Levi CG. Materials design for the next generation thermal barrier coatings. *Ann Rev Mater Res* 2003;33:383–417.
- [16] Cao XQ, Vassen R, Stöver D. Ceramic materials for thermal barrier coatings. *J Eur Ceram Soc* 2004;24.
- [17] Karlsson AM, Hutchinson JW, Evans AG. The displacement of the thermally grown oxide in thermal barrier systems upon temperature cycling. *Mater Sci Eng* 2003;A351:244–57.
- [18] He MY, Hutchinson JW, Evans AG. Simulation of stresses and delamination in a plasma sprayed thermal barrier system upon thermal cycling. *Mater Sci Eng* 2003;A345:172–8.
- [19] Schlichting KW, Padture NP, Jordan EH, Gell M. Failure modes in plasma sprayed thermal barrier coatings. *Mater Sci Eng* 2003; A342:120–30.
- [20] Busso EP, Lin J, Sakurai S. A mechanistic study of oxidation-induced degradation in a plasma sprayed thermal barrier coating system. Part II: life prediction model. *Acta Mater* 2001;49:1529–36.
- [21] Vassen R, Kerkhoff G, Stöver D. Development of a micromechanical life prediction model for plasma sprayed thermal barrier coatings. *Mater Sci Eng* 2001;A303:100–9.
- [22] Chen X, Hutchinson JW, He MY, Evans AG. On the propagation and coalescence of delamination cracks in compressed coatings: with application to thermal barrier systems. *Acta Mater* 2003;51: 2017–30.
- [23] Karlsson AM, Xu T, Evans AG. The displacement instability transition in thermal barrier systems. *Acta Mater* 2002;50:1211–8.
- [24] Mumm DR, Evans AG, Spitsberg IT. Characterization of a cyclic displacement instability for a thermally grown oxide in a thermal barrier system. *Acta Mater* 2001;49:2329–40.
- [25] Karlsson AM, Levi CG, Evans AG. A model study of displacement instabilities during cyclic oxidation. *Acta Mater* 2002;50: 1263–73.
- [26] Ambrico JM, Begley MR, Jordan EH. Stress and shape evolution of irregularities in oxide films on elastic–plastic substrates due to thermal cycling and film growth. *Acta Mater* 2001;49:1577–88.
- [27] Tolpygo VK, Clarke DR. Surface rumpling of a (Ni,Pt)Al bond coat induced by cyclic oxidation. *Acta Mater* 2000;48:3283–93.
- [28] Chen MW, Ott RT, Hufnagel TC, Wright PK, Hemker KJ. Microstructural evolution of platinum modified nickel aluminide bond coat during thermal cycling. *Surf Coat Technol* 2003;163–164:2–30.
- [29] Clarke DR. Stress generation during high-temperature oxidation of metallic alloys. *Curr Opin Solid State Mater Sci* 2002;6:237–44.
- [30] Bisson J-F, Fournier D, Poulain M, Lavigne O, Mévrel R. Thermal conductivity of yttria–zirconia single crystals, determined with spatially resolved infrared thermography. *J Am Ceram Soc* 2000;83:1993–8.
- [31] Mévrel R, Laizet JC, Azzopardi A, Leclercq B, Poulain M, Lavigne O, Demange D. Thermal diffusivity and conductivity of  $Zr_{1-x}Y_xO_{2-x/2}$  ( $x = 0, 0.084$  and  $0.179$ ) single crystals. *J. Eur. Ceram. Soc.* (in press).
- [32] Stecura S. Optimization of the NiCrAl–Y/ZrO<sub>2</sub>–Y<sub>2</sub>O<sub>3</sub> thermal barrier system NASA Report No. TM-86905. NASA, Cleveland, OH; 1985.
- [33] Miller RA, Smialek JL, Garlick RG. Phase stability in plasma-sprayed, partially stabilized zirconia–yttria. In: Heuer AH, Hobbs LW, editors. Science and technology of zirconia. Advances in ceramics, vol. 3. The American Ceramic Society, Inc; 1981. p. 241–53.
- [34] Jones RL, Mess D. Improved tetragonal phase stability at 1400 °C with scandia, yttria-stabilized zirconia. *Surf Coat Technol* 1996;86–87:94–101.
- [35] Yanar NM, Stiger MJ, Maris-Sida M, Pettit FS, Meier GH. The effects of high temperature exposure on the durability of thermal barrier coatings. *Key Eng Mater* 2001;197:145–63.
- [36] Vassen R, Czech N, Mallener W, Stamm W, Stöver D. Influence of impurity content and porosity of plasma sprayed yttria stabilized zirconia layers on the sintering behavior. *Surf Coat Technol* 2001;141:135–40.
- [37] Azzopardi A, Mévrel R, Saint-Ramond B, Olson E, Stiller K. Influence of aging on structure and thermal conductivity of Y-PSZ and Y-FSZ EB-PVD coatings. *Surf Coat Technol* 2004;177–178:131–9.
- [38] Dinwiddie RB, Beecher SC, Porter WD, Nagaraj BA. The effect of thermal aging on the thermal conductivity of plasma sprayed and EB-PVD thermal barrier coatings. ASME Report 96-GT-282, American Society of Mechanical Engineers; 1996.
- [39] Wellman RG, Nicholls JR. On the effect of ageing on the erosion of EB-PVD TBCs. *Surf Coat Technol* 2004;177–178:80–8.
- [40] Chen X, He MY, Spitsberg IT, Fleck NA, Hutchinson JW, Evans AG. Mechanisms governing the high temperature erosion of thermal barrier coatings. *Wear* (in press).
- [41] Wellman RG, Nicholls JR. A mechanism for the erosion of EB PVD TBCs. *Mater Sci Forum* 2001;369–372:531–8.
- [42] Chen X, Wang R, Yao N, Evans AG, Hutchinson JW, Bruce RW. Foreign object damage in a thermal barrier system: mechanisms and simulations. *Mater Sci Eng* 2003;A352:221–31.

- [43] Darolia R, Nagaraj BA. Method of forming a coating resistant to deposits and coating formed thereby. US Patent Application, US 2003/0152797 A1; 2003.
- [44] Borom MP, Johnson CA, Peluso LA. Role of environmental deposits and operating surface temperature in spallation of air plasma sprayed thermal barrier coatings. *Surf Coat Technol* 1996;86–87:116–26.
- [45] Marple BR, Voyer J, Moreau C, Nagy DR. Corrosion of thermal barrier coatings by vanadium and sulfur compounds. *Mater High Temper* 2000;17:397–412.
- [46] Leyens C, Wright IG, Pint BA. Hot corrosion of an EB-PVD thermal-barrier coating system at 950 °C. *Oxidat Metals* 2000;54:401–24.
- [47] Jones RL, Reidy RF, Mess D. Scandia, yttria-stabilized zirconia for thermal barrier coatings. *Surf Coat Technol* 1996;82:70–6.
- [48] Nicholls JR, Deakin MJ, Rickerby DS. A comparison between the erosion behavior of thermal spray and electron-beam physical vapour deposition thermal barrier coatings. *Wear* 1999;233–235:352–61.
- [49] Nicholls JR, Lawson KJ, Rickerby DS, Morell P. Advanced processing of TBCs for reduced thermal conductivity. In: *Proceedings of the 85th Meeting of the AGARD Structures and Materials Panel*; Aalborg, Denmark: AGARD (Advisory Group for Aerospace Research and Development); 1998. p. 6.1–9.
- [50] Rigney DV, Maricocchi AF, Wortman DJ, Bruce RW, Rigney JD. Method for forming a thermal barrier coating system. US Patent, 6,447,854; 2002.
- [51] Rigney JD, Wortman DJ. Physical properties of thermal barrier coatings using electron beam-physical vapor deposition. US Patent, 6,620,465; 2003.
- [52] Jaslier YP, Malle AHL, Huchin J-P, Alperine S, Portal R. Ceramic heat barrier coating having low thermal conductivity and process for the deposition of said coating. US Patent, 6,251,504 B1; 2001.
- [53] Marijnissen GH, van Lieshout AHF, Ticheler GJ, Bons HJM, Ridder ML. Thermal barrier coating system ceramic structure. US Patent, 5,876,860; 1999.
- [54] Strangman TE. Thermal barrier coatings for turbine airfoils. *Thin Solid Films* 1985;127:93–105.
- [55] Hass D, Parrish PA, Wadley HNG. Electron beam directed vapor deposition of thermal barrier coatings. *J Vacuum Sci Technol A* 1998;16:3396–401.
- [56] Hass DD, Slifka AJ, Wadley HNG. Low thermal conductivity vapor deposited zirconia microstructures. *Acta Mater* 2001;49:973–83.
- [57] Préaucht B, Drawin S, Landais S. Performances of a microwave PECVD reactor for thin or thick oxide coatings at extremely high deposition rate. In: *Proceedings of the Society of Vacuum Coaters 44th Annual Technical Conference*. Philadelphia, PA: Society of Vacuum Coaters; 2001.
- [58] Bertrand G, Mévrel R. Zirconia coatings realized by microwave plasma-enhanced chemical vapor deposition. *Thin Solid Films* 1997;292:241–6.
- [59] Préaucht B, Drawin S. Isothermal and cycling properties of zirconia-based thermal barrier coatings deposited by PECVD. *Surf Coat Technol* 2001;146–147:94–101.
- [60] Taylor TA. Thermal barrier coating for substrates and process for producing it. US Patent, 5,073,433; 1991.
- [61] Kokini K, Banerjee A, Taylor TA. Thermal fracture of interfaces in pre-cracked thermal barrier coatings. *Mater Sci Eng* 2002;A323:70–82.
- [62] Farmer G. Method of protecting gas turbine combustor components against water erosion and hot corrosion. US Patent, 6,047,539; 2000.
- [63] Bruce RW, Schaeffer JC. Sprayed ZrO<sub>2</sub> thermal barrier coating with vertical cracks. European Patent, EP1281788; 2003.
- [64] Graham SD, DeSol MF, Smith ML, Wallace MW, Ling RL. Dense vertically cracked thermal barrier coating process to facilitate post-coat surface finishing. US Patent, 6,432,487; 2000.
- [65] Platts: Top Plants 2003: Baglan Bay Power Station. *Power* 2003;147:45–8.
- [66] Padture NP, Schlichting KW, Bhatia T, Ozturk A, Cetegen B, Jordan EH, et al. Toward durable thermal barrier coatings with novel microstructures deposited by solution precursor plasma spray. *Acta Mater* 2001;49:2251–7.
- [67] Bhatia T, Ozturk A, Xie L, Jordan EH, Cetegen B, Gell M, et al. Mechanisms of ceramic coating deposition in solution precursor plasma spray. *J Mater Res* 2002;17:2363–72.
- [68] Gell M, Xie L, Ma X, Jordan EH, Padture NP. Highly durable thermal barrier coatings made by the solution precursor plasma spray process. *Surf Coat Technol* 2004;177–178:97–102.
- [69] Terry SG. Evolution of microstructure during the growth of thermal barrier coatings by electron-beam physical vapor deposition. Doctoral Dissertation in Materials. University of California, Santa Barbara, CA; 2001.
- [70] Wadley HNG, Zhou XW, Johnson RN, Neurock M. Mechanisms, models and methods of vapor deposition. *Progr Mater Res* 2001;46:329–77.
- [71] Cho J, Terry SG, LeSar R, Levi CG. A kinetic Monte Carlo simulation of film growth by physical vapor deposition on rotating substrates. *Mater Sci Eng* (submitted).
- [72] Schulz U, Terry SG, Levi CG. Microstructure and texture of EB-PVD TBCs grown under different rotation modes. *Mater Sci Eng* 2003;A360:319–29.
- [73] Kulkarni A, Wang Z, Nakamura T, Sampath S, Goland A, Herman H, et al. Comprehensive microstructural characterization and predictive property modeling of plasma sprayed zirconia coatings. *Acta Mater* 2003;51:2457–75.
- [74] Yokokawa H, Sakai N, Kawada T, Dokiya M. Phase diagram calculations for ZrO<sub>2</sub> based ceramics: thermodynamic regularities in zirconate formation and solubilities of transition metal oxides. In: Badwal SPS, Bannister MJ, Hannink RHJ, editors. *Science and technology of zirconia V*. Technomic Publishing; 1990. p. 59–68.
- [75] Leclercq B, Mévrel R. Thermal conductivity of zirconia-based ceramics for thermal barrier coatings. In: *10th International Ceramics Congress (CIMTEC)* July 14–19, 2002, Firenze, Italy; 2002. p. 365–72.
- [76] Nicholls JR, Lawson KJ, Johnstone A, Rickerby DS. Methods to reduce the thermal conductivity of EB-PVD TBCs. *Surf Coat Technol* 2002;151–152:383–91.
- [77] Zhu D, Miller RA. Thermal conductivity and sintering behavior of advanced thermal barrier coatings. *Ceram Eng Sci Proc* 2002;23:457–68.
- [78] Zhu D, Chen YL, Miller RA. Defect clustering and nano-phase structure characterization of multi-component rare earth oxide doped zirconia-yttria thermal barrier coatings. *Ceram Eng Sci Proc* 2003;24:525–34.
- [79] Rigney JD, Darolia R. Yttria-stabilized zirconia with reduced thermal conductivity. US Patent, US 6,586,115 B2; 2003.
- [80] Maloney MJ. Thermal barrier coating systems and materials. US Patent, 6,117,560; 2000.
- [81] Maloney MJ. Thermal barrier coating systems and materials. European Patent Application, EP 0 992 603 A1; 2000.
- [82] Vassen R, Cao X, Tietz F, Basu D, Stöver D. Zirconates as new materials for thermal barrier coatings. *J Am Ceram Soc* 2000;83:2023–8.
- [83] Wu J, Wei X, Padture NP, Klemens PG, Gell M, Garcia E, et al. Low-thermal-conductivity rare-earth zirconates for potential thermal barrier coating applications. *J Am Ceram Soc* 2002;85:3031–5.
- [84] Maloney MJ. Thermal barrier coating systems and materials. US Patent Application, 20030049470 A1; 2003.



- [85] Zhu D, Miller RA. Thermal conductivity and elastic modulus evolution of thermal barrier coatings under high heat flux conditions. *J Therm Spray Technol* 2000;9:175–80.
- [86] Clarke DR. Materials selection guidelines for low thermal conductivity thermal barrier coatings. *Surf Coat Technol* 2003; 163–164:67–74.
- [87] Klemens PG. The scattering of low-frequency lattice waves by static imperfections. *Proc Phys Soc London* 1955;A68:1113–28.
- [88] Suresh G, Seenivasan G, Krishnaiah MV, Murti PS. Investigation of the thermal conductivity of selected compounds of gadolinium and lanthanum. *J Nucl Mater* 1997;249:259–61.
- [89] Suresh G, Seenivasan G, Krishnaiah MV, Murti PS. Investigation of the thermal conductivity of selected compounds of lanthanum, samarium and europium. *J Alloys Compd* 1998;269: L9–L12.
- [90] Maloney MJ. Thermal barrier coating systems and materials. US Patent, 6,177,200; 2001.
- [91] Lehmann H, Pitzer D, Pracht G, Vassen R, Stöver D. Thermal conductivity and thermal expansion coefficient of the lanthanum rare-earth element zirconate system. *J Am Ceram Soc* 2003;86: 1338–44.
- [92] Subramanian R. Thermal barrier coating having high phase stability. US Patent, 6,258,467; 2001.
- [93] Wu J, Padture NP, Klemens PG, Gell M, Garcia E, Miranzo P, et al. Thermal conductivity of ceramics in the  $\text{ZrO}_2\text{--GdO}_{1.5}$  system. *J Mater Res* 2002;17:3193–200.
- [94] Fevre M. Etudes microstructurales d'oxydes desordonnes et modelisation de leurs proprietes thermiques. Doctoral Dissertation in Science. Universite de Parix XI Orsay; 2003.
- [95] Vassen R, Lehmann H, Dietrich M, Cao X, Stöver D, Pracht G. Heat-insulating layer based on  $\text{La}_2\text{Zr}_2\text{O}_7$  for high temperatures. International Patent Application, WO 02081768 A2; 2002.
- [96] Maloney MJ, Achter HS, Barkalow RH. Development of ceria-base low thermal conductivity thermal barrier coatings. In: Cincinnati OH, Brindley WJ, editors. Proceedings of the 1997 Thermal Barrier Coating Workshop, NASA Lewis Research Center; 1997.
- [97] Maloney MJ. Article having a durable ceramic coating. US Patent, 6,187,453; 2001.
- [98] Cao X, Vassen R, Fischer W, Tietz F, Jungen W, Stöver D. Lanthanum–cerium oxide as a thermal barrier coating material for high temperature applications. *Adv Mater* 2003;15:1438–41.
- [99] Friedrich CJ, Gadow R, Schirmer T. Lanthanum hexaaluminate—a new material for atmospheric plasma spraying of advanced thermal barrier coatings. *J Therm Spray Technol* 2001;10:592–8.
- [100] Gadow R, Lischka MH. Lanthanum hexaluminate—novel thermal barrier coatings for gas turbine applications—materials and process development. *Surf Coat Technol* 2002;151:392–9.
- [101] Saruhan-Brings B, Schulz U, Kröder CJ. Thermal insulating material with an essentially magnetoplumbitic crystal structure. European Patent Application, EP 1256636 A2; 2002.
- [102] Padture NP, Klemens PG. Low thermal conductivity in garnets. *J Am Ceram Soc* 1997;80:1018–20.
- [103] Sudre O, Cheung J, Marshall D, Morgan P, Levi CG. Thermal insulation coatings of  $\text{LaPO}_4$ . *Ceram Eng Sci Proc* 2001;22:367–74.
- [104] Klemens PG, Gell M. Thermal conductivity of thermal barrier coatings. *Mater Sci Eng* 1998;A245:143–9.
- [105] Schelling PK, Phillpot SR, Grimes RW. Optimum pyrochlore compositions for low thermal conductivity. *Philos Mag Lett* 2003;84:127–37.
- [106] Slack GA. The thermal conductivity of non-metallic crystals. *Solid State Phys* 1979;34:1–71.
- [107] Cahill DG, Watson SK, Pohl RO. Lower limit to the thermal conductivity of disordered crystals. *Phys Rev B—Cond Matter* 1992;46:6131–40.
- [108] Levi CG. Metastability and microstructure evolution in the synthesis of inorganics from precursors. *Acta Mater* 1998;46:787–800.
- [109] Mennicke C, Mumm DR, Clarke DR. Transient phase evolution during oxidation of a two-phase NiCoCrAlY bond coat. *Zeit Metal* 1999;90:1079–84.
- [110] Tolpygo VK, Clarke DR. Microstructural study of the theta-to-alpha transformation in alumina scales formed on nickel-aluminides. *Mater High Temp* 2000;17:59–70.
- [111] Levi CG, Sommer E, Terry SG, Catanoiu A, Rühle M. Alumina grown during deposition of thermal barrier coatings on NiCrAlY. *J Am Ceram Soc* 2002;86:676–85.
- [112] Leckie RMR, Rebollo NR, Yang JY, Levi CG. Microstructure stability issues in emerging TBC materials. In: Kaysser WA, editor. Proceedings of an International Symposium on Thermal Barrier Coatings and Titanium Aluminides for Gas Turbines (TurbOMat), Bonn, Germany, DLR; 2002.
- [113] Fabrichnaya O, Aldinger F. Assessment of the thermodynamic parameters in the system  $\text{ZrO}_2\text{--Y}_2\text{O}_3\text{--Al}_2\text{O}_3$ . *Zeit Metal* 2004;95: 27–39.
- [114] Dietrich M, Vassen R, Cao X, Stöver D. Combined heat insulating layer systems. US Patent Application, US 2003/ 0148148 A1; 2003.
- [115] Subramanian R. Highly defective oxides as sinter resistant thermal barrier coating. US Patent Application, US 203/ 0108768; 2003.
- [116] Miller RA. Thermal barrier coatings for aircraft engines: history and directions. *J Therm Spray Technol* 1997;6:35–42.
- [117] Stecura S. New  $\text{ZrO}_2\text{--Yb}_2\text{O}_3$  plasma-sprayed coatings for thermal barrier applications. *Thin Solid Films* 1987;150:15–40.
- [118] Ibégazène H, Alperine S, Diot C. Yttria stabilized hafnia-zirconia thermal barrier coatings: influence of hafnia addition on TBC structure and high temperature behavior. In: Ceramic coatings. ASME-MD; 1993. p. 173–95.
- [119] Zhu D, Nesbitt JA, McCue TR, Barrett CA, Miller RA. Furnace cyclic behavior of plasma-sprayed Zirconia-Yttria and multi-component rare earth oxide doped thermal barrier coatings. *Ceram Eng Sci Proc* 2002;23:533–45.
- [120] Sasaki K, Bohac P, Gauckler LJ. Phase equilibria in the system  $\text{ZrO}_2\text{--InO}_{1.5}$ . *J Am Ceram Soc* 1994;76:689–98.
- [121] Yashima M, Kakihana M, Yoshimura M. Metastable-stable phase diagrams in the zirconia-containing systems utilized in solid-oxide fuel cell application. *Solid State Ion* 1996;86–88:1131–49.
- [122] Katamura J, Seki T, Sakuma T. The cubic-tetragonal phase equilibria in the  $\text{ZrO}_2\text{--R}_2\text{O}_3$  ( $\text{R} = \text{Y, Gd, Sm, Nd}$ ) systems. *J Phase Equilib* 1995;16:315–9.
- [123] Bastide B, Odier P, Coutures JP. Phase equilibrium and martensitic transformation in lanthana-doped zirconia. *J Am Ceram Soc* 1988;71:449–53.
- [124] Jones RL. Scandia, yttria-stabilized zirconia for ultra-high temperature thermal barrier coatings. US Patent, 6,044,830; 2000.
- [125] Rebollo NR, Fabrichnaya O, Levi CG. Phase stability of Y + Gd co-doped zirconia. *Zeit Metal* 2003;94:163–70.
- [126] Singheiser L, Steinbrech RW, Quadakkers WJ, Herzog R. Failure aspects of thermal barrier coatings. *Mater High Temp* 2001;18:249–59.
- [127] Watanabe M, Mercer C, Levi CG, Evans AG. A probe for the high temperature deformation of oxides used for thermal barrier systems. *Acta Mater* 2004;52:1479–87.
- [128] Darolia R. Thermal barrier coating with improved erosion and impact resistance. US Patent, 6,617,049; 2003.

- [129] Rigney JD, Darolia R. Thermal barrier coating with improved erosion and impact resistance and process therefore. US Patent, US 6,620,525 B1; 2003.
- [130] Bruce RW, Schaeffer JC, Rosenzweig MA, Viguie R, Rigney DV, et al. Thermal barrier coating resistant to erosion and impact by particulate matter. US Patent, 5,683,825; 1997.
- [131] Schulz U, Peters M, Bach F-W, Tegeder G. Graded coatings for thermal, wear and corrosion barriers. *Mater Sci Eng* 2003;A362: 61–80.
- [132] Bruce RW, Burlingame NH. Article protected by thermal barrier coating having a sintering inhibitor, and its fabrication. US Patent Application, US 2003/0077477 A1; 2003.
- [133] Subramanian R. In situ formation of multiphase electron beam physical vapor deposited barrier coatings for turbine components. US Patent, US 6,296,945 B1; 2001.
- [134] Raybould D, Strangman TE, Fischer WE, Chipko PA. Thermal barrier coating with alumina bond inhibitor. US Patent, 6,103,386; 2000.
- [135] Hasz WC, Borom MP, Johnson CA. Protection of thermal barrier coating with an impermeable barrier coating. US Patent, 5,871,820; 1999.
- [136] Stowell WR, Nagaraj BA, Lee CP, Ackerman JF, Israel RS. Enhanced coating system for turbine airfoil applications. US Patent, US 6,394,755 B1; 2002.
- [137] Bruce RW, Rosenzweig MA, Schaeffer JC, Wortman DJ. Method for forming a multilayer thermal barrier coating. US Patent, 6,054,184; 2000.
- [138] Mullin RS, Allen WP, Gell ML, Barkalow RH, Noetzel AA, Appleby JW, et al. Multiple nanolayer coating system. US Patent, 5,687,679; 1997.
- [139] An K, Ravichandran KS, Dutton RE, Semiatin SL. Microstructure, texture, and thermal conductivity of single-layer and multilayer thermal barrier coatings of  $Y_2O_3$ -stabilized  $ZrO_2$  and  $Al_2O_3$  made by physical vapor deposition. *J Am Ceram Soc* 1999; 82:399–406.
- [140] Krell T, Schulz U, Peters M, Kaysser WA. Graded EB-PVD alumina–zirconia thermal barrier coatings—an experimental approach. *Mater Sci Forum* 1999;308–311:396–401.
- [141] Maloney MJ. Ceramic coatings containing layered porosity. US Patent, 6,057,047; 2000.
- [142] Strangman TE. Porous thermal barrier coating. US Patent, 5,512,382; 1996.
- [143] Strangman TE, Raybould D. Lower conductivity barrier coating. US Patent, US 6,482,537 B1; 2002.
- [144] Stowell WR, Ackerman JF, Skoog AJ, Cook GE, Varney GE. Multilayer dielectric stack coated part for contact with combustion gases. US Patent, 5,851,679; 1998.
- [145] Skoog AJ, Murphy JA, Stowell WR. Article with a diffuse reflective barrier coating and a low emissivity coating thereon, and its preparation. US Patent, US 6,210,791 B1; 2001.
- [146] Allen WP, Veronesi WA, Hall RJ, Maloney MJ, Appleby JW, Hague DC, et al. Reflective coatings to reduce radiation heat transfer. US Patent, US 6,652,987 B2; 2003.
- [147] Feist JP, Heyes AL, Nicholls JR. Phosphor thermometry in an electron beam physical vapour deposition produced thermal barrier coating doped with dysprosium. *Proc Inst Mech Eng, Part G J Aerospace Eng* 2001;215:333–41.
- [148] Feist JP, Heyes AL, Seefelt S. Thermographic phosphor thermometry for film cooling studies in gas turbine combustors. *Proc Inst Mech Eng, Part A: J Power Energy* 2003;217:193–200.
- [149] Tolpygo VK, Clarke DR, Murphy KS. The effect of grit blasting on the oxidation behavior of a platinum-modified nickel–aluminide coating. *Metall Mater Trans A* 2001;32A:1467–78.
- [150] Tolpygo VK, Clarke DR, Murphy KS. Oxidation-induced failure of EB-PVD thermal barrier coatings. *Surf Coat Technol* 2001;146–147:124–31.
- [151] Yanar NM, Meier GH, Pettit FS. The influence of platinum on the failure of EBPVD YSZ TBCs on NiCoCrAlY bond coats. *Scri Mater* 2002;46:325–30.
- [152] Clarke DR, Sergo V, He MY. Precursor to TBC failure caused by constrained phase transformation in the thermally grown oxide. In: Hampikian JM, Dahotre NB, editors. *Elevated temperature coatings: science and technology, III. The Minerals, Metals and Materials Society*; 1999. p. 67–78.
- [153] Schaeffer JC, Connor WB, Field RD. Method for forming a thermal barrier coating. US Patent, 6,123,997; 2000.
- [154] Spitsberg IT. Method for improving the TBC life of a single phase platinum aluminide bond coat by preoxidation heat treatment. US Patent Application, US 2003/0203221 A1; 2003.
- [155] Pan D, Chen MW, Wright PK, Hemker KJ. Evolution of a diffusion aluminide bond coat for thermal barrier coatings during thermal cycling. *Acta Mater* 2003;51:2205–17.
- [156] Rigney JD, Darolia R, Walston WS, Corderman RR. Nickel aluminide coating and coating systems formed therewith. US Patent, 6,153,313; 2000.
- [157] Darolia R. Bond coat for a thermal barrier coating and method thereof. US Patent, US 6,255,001 B1; 2001.
- [158] Darolia R, Rigney JD, Grylls RJ. Nickel aluminide alloys with Cr and Zr for adherent coating or interlayer on superalloy turbine parts. US Patent, US 6,291,084 B1; 2001.
- [159] Darolia R, Rigney JD, Pfandtner JA. Nickel aluminide coating and coating systems formed therewith. US Patent Application, US 2003/0118863 A1; 2003.
- [160] Saint Ramond B, Nicholls JR. Method of making a protective coating forming a thermal barrier with bonding underlayer on a superalloy substrate, and a part obtained thereby. US Patent, US 6,645,351 B2; 2003.
- [161] Spitsberg IT, Darolia R, Jackson MR, Zhao J-C, Schaeffer JC. Diffusion barrier layer. US Patent, US 6,306,524 B1; 2001.
- [162] Tryon B, Pollock TM, Gigliotti MFX, Hemker K. Thermal expansion behavior of ruthenium aluminides. *Scri Mater* 2004; 50:845–8.
- [163] Zhao J-C, Jackson MR, Grylls RJ, Darolia R. Heat-resistant Ru alloy coating for protection of superalloy substrates in high temperature. US Patent Application, US 2003148141 A1; 2003.
- [164] Zhao J-C, Jackson MR. Diffusion interlayer for barrier coating on superalloy articles. US Patent Application, US 2002197502; 2002.
- [165] Zhao J-C, Jackson MR. Gas-turbine parts and similar articles precoated with Pt-group alloys for high temperature service. European Patent, EP 1347079; 2003.
- [166] Yokokawa H, Sakai N, Kawada T, Dokiya M. Chemical potential diagrams for rare earth-transition metal-oxygen systems: I, Ln–V–O, Ln–Mn–O systems. *J Am Ceram Soc* 1990;73: 649–58.
- [167] Murphy KS. Stabilized Zirconia thermal barrier coating with Hafnia. US Patent Application, US 2003/0118873 A1; 2003.
- [168] Rebollo NR, Gandhi AS, Levi CG. Phase stability issues in emerging TBC systems. In: Opila EJ, Hou P, Maruyama T, Pieraggi B, McNallan M, Shifer D, Wuchina E, editors. *High Temperature Corrosion and Materials Chemistry IV. Electrochemical Society Proceedings*, vol. PV-2003-16;2003. p. 431–42.

**This Page is Inserted by IFW Indexing and Scanning  
Operations and is not part of the Official Record**

**BEST AVAILABLE IMAGES**

Defective images within this document are accurate representations of the original documents submitted by the applicant.

Defects in the images include but are not limited to the items checked:

- ☐ **BLACK BORDERS**
- ☐ **IMAGE CUT OFF AT TOP, BOTTOM OR SIDES**
- ☒ **FADED TEXT OR DRAWING**
- ☒ **BLURRED OR ILLEGIBLE TEXT OR DRAWING**
- ☐ **SKEWED/SLANTED IMAGES**
- ☐ **COLOR OR BLACK AND WHITE PHOTOGRAPHS**
- ☐ **GRAY SCALE DOCUMENTS**
- ☐ **LINES OR MARKS ON ORIGINAL DOCUMENT**
- ☐ **REFERENCE(S) OR EXHIBIT(S) SUBMITTED ARE POOR QUALITY**
- ☐ **OTHER:** \_\_\_\_\_

**IMAGES ARE BEST AVAILABLE COPY.**

**As rescanning these documents will not correct the image problems checked, please do not report these problems to the IFW Image Problem Mailbox.**